Stability of rigid motions and coating films in bicomponent flows of immiscible liquids

By DANIEL D. JOSEPH AND LUIGI PREZIOSI

Department of Aerospace Engineering and Mechanics, 107 Akeman Hall, University of Minnesota, 110 Union Street S.E., Minneapolis, MN 55455, USA

We consider the problem of global stability of the rigid rotation of two fluids. The realized interfacial configurations minimize a potential. We derive the most general form of the potential in which the working of the contact line may be expressed as a potential. The resulting variational problem for the interfacial potential is solved when the contact-line conditions are prescribed and for coating flows in which the interface makes a tangent contact with the wetted rod. In the former case, good agreement with experiments is obtained except near lines of contact. This shows that a spinning rod interfacial tensiometer is viable. In the latter case of coating flow, we get good agreement with experiments when the effects of gravity are not too large. The problem of bifurcation of coating flow is discussed qualitatively and some experimental results are given. We show how bifurcating sequences fit well into our qualitative description of the solution which must minimize the interfacial potential as the angular velocity is increased. The last bifurcations lead to pendant drops on a rotating 'ceiling' under the influence of centripetal forces which replace gravity. The dynamics of rollers of oil in water, or part in water and part in air, are explained in terms of the wavelength dependence of rotating drops.

1. Introduction. The problem of placements and the problem of shapes

Flows of two fluids are important and interesting because they are commonplace, they lend themselves to technological applications and they introduce new phenomena without counterpart in the flow of one fluid.

Many configurations of flow of two fluids are possible. We see layers, slugs, rollers, sheets, bubbles, drops and emulsions and foams (see Joseph, Nguyen, Beavers 1984, 1986, hereinafter referred to as JNB). These structures are often topologically different from the rest configurations from which they arise. The evolution involves breakup of liquids, a process which is not included in the usual statements governing dynamics (say, the Navier–Stokes equations). In some approximate sense, the configurations and the flow of two fluids that are ultimately achieved in practice are controlled by the problem of placements and the problem of shapes. In the problem of placements, we must describe the massive transport required to position the two fluids in the places they ultimately occupy. This problem is controlled by fingering flows and breakup and frequently is such that the low-viscosity constituent is found in the regions of high shear. Some suggestive ideas about the sets of solutions of the problem of placements that may be realized in practice can be determined by arranging the liquids to minimize the dissipation. Actually different minimum problems can be imagined (see JNB) and probably none of them are precise statements of what dynamics will allow. It may in fact be more useful to express the

type of 'minimization' achieved by the fluids in the anthropomorphic terms used by JNB: 'High viscosity liquids hate to work. Low viscosity liquids are the victims of the laziness of high viscosity liquids because they are easy to push around'.

The problem of shapes has to do with the geometric form of the interfaces between flowing fluids. This problem involves surface tension and other potential terms which enter into each problem. The problem of shapes for rigid rotations of two fluids was considered by Joseph *et al.* (1985, hereinafter referred to as JRRN). This paper extends and solves the problem of shapes posed by them.

The problem of placements can be framed as a variational problem for configurations which minimize a dissipation. This variational problem is perhaps a suggestive but not exact statement of the placements allowed by dynamics. The problem of shapes can also be framed as a variational problem. In this problem we seek the shapes that minimize a potential energy. In general this variational problem is also merely suggestive but in some limits it is also exact. The problem of rigid rotations of two fluids without gravity is one of these special cases in which the shape of the interface may be determined by minimizing a potential.

2. Energy theory of stability of rigid motions of two fluids with contact lines

2.1. *Steady rigid rotation of two fluids*

Rigid motions of a fluid are possible provided that the fluid rotates steadily about a fixed axis. Drops, bubbles, different types of fluids in all types of containers may rotate rigidly. Various kinds of perturbations of rigid motion are also of interest.

A single liquid which fills a container rotating steadily around some fixed axis will eventually rotate with the container. But in the case of two fluids it is necessary to determine the places occupied by the two fluids and the shape of the interfaces.

We shall consider the special case in which the two liquids occupy the region

$$G = \{x = (r, \theta, x) \mid R_1 < r < R_2, \quad 0 \leqslant \theta < 2\pi, \quad -\Lambda < x < \Lambda\}$$

between two coaxial cylinders of radius R_1 and R_2 which rotate with a common angular velocity Ω. The reader will see that this special choice of domain is required for only some of our results. Liquid one is in G_1 and two is in G_2, $G_1 \cup G_2 = G$. The interface between G_1 and G_2 is called Σ. It may be of disjoint parts. Jumps across Σ are designated by $[\cdot] = (\cdot)_1 - (\cdot)_2$.

Candidates for rigid motions, with gravity neglected, are

$$(u_0, p_0) = (\Omega r e_\theta, \tfrac{1}{2}\rho \Omega^2 r^2 + c). \tag{2.1}$$

The velocity is continuous across Σ no matter what Σ, and the excess stress vanishes. We call (2.1) a candidate because it need not satisfy the normal-stress condition

$$[p_0] = -2HT \quad \text{on } \Sigma, \tag{2.2}$$

$$[p_0] = [\rho]\tfrac{1}{2}\Omega^2 R^2 + [c] \tag{2.3}$$

where R is the value of r at a point on Σ and $2H$ is the sum of the principal curvatures. Expressions for $2H$ in cylindrical coordinates are given in JRRN.

The dynamical effects of gravity are negligible whenever secondary motions induced by gravity are small. We may absorb gravity into $\phi = p + \rho g r \sin \theta$ in the equation of motion. There will be no secondary motions if ϕ is independent of θ. Of

course, p must then depend on θ, at least like $\sin \theta$. This is compatible with the normal stress condition

$$-[\phi]+[\rho]gR \sin \theta+[S_{nn}]+2HT = 0$$

if $[\phi] = [p_0], [S_{nn}] = 0$ and

$$\frac{[p_0]}{[\rho gd]} = \frac{\Omega^2 d}{2g} = F^2 \gg 1 \,, \tag{2.4}$$

where F is a Froude number and $d = \bar{R}$ is the mean value of $R(\theta, x) = R(x)$. The effects of terrestrial gravity are dominated by centrifugal 'gravity' when the Froude number is large.

There is another situation in which the dynamical effects of gravity are negligible which is easiest to understand as the rigid motion of thin coating films of very viscous liquids. In this case it is p that is independent of θ and secondary motions are suppressed by the fact that the force of gravity is not sufficient to make a thin viscous liquid flow. The criterion for this, derived for thin films rotating in air, is

$$\frac{gD_0^2}{\nu \Omega a} \ll 1 \,, \tag{2.5}$$

where D_0 is the maximum film thickness and ν is kinematic viscosity of the liquid.

We shall now proceed with $g = 0$.

2.2. *Disturbance equations*

Set

$$\left.\begin{aligned} u &= u_0+\hat{u} \,, \\ p &= p_0+\hat{p} \,. \end{aligned}\right\} \tag{2.6}$$

Then

$$\rho \left[\frac{\partial \hat{u}}{\partial t}+\hat{u}\cdot\nabla u_0+u_0\cdot\nabla\hat{u}+\hat{u}\cdot\nabla\hat{u}\right] = -\nabla\hat{p}+\mathrm{div}\,\hat{S} \,, \tag{2.7}$$

where $\hat{u}$ is solenoidal and satisfies the no-slip condition on the cylinder walls. At the interface Σ

$$\left.\begin{aligned} [\hat{u}] &= O \,, \\ -[\hat{p}]\,n+[\hat{S}]\cdot n &= [p_0]\,n+2HTn \,. \end{aligned}\right\} \tag{2.8}$$

For any integrable function f which is equal to f_1 in G_1 and f_2 in G_2, we define

$$\langle f \rangle = \int_{G_1} f_1 \,\mathrm{d}x + \int_{G_2} f_2 \,\mathrm{d}x \,. \tag{2.9}$$

For any g defined on Σ we define

$$\langle g \rangle_\Sigma = \int_\Sigma g \,\mathrm{d}\Sigma \,. \tag{2.10}$$

Since the total volume of each incompressible fluid is conserved, we deduce that

$$\langle u\cdot n \rangle_\Sigma = 0 \,. \tag{2.11}$$

If Σ is given by $\quad F(x(t), t) = 0 \,,$

then

$$\frac{\mathrm{d}F}{\mathrm{d}t} = \frac{\partial F}{\partial t}+u\cdot\nabla F = 0 \,, \tag{2.12}$$

where we have assumed that the normal component of the velocity $\mathrm{d}x/\mathrm{d}t$ of the surface $\varSigma$ and the particles of fluids on either side of $\varSigma$ are the same. In fact, the velocity $\boldsymbol{u}$ is continuous across $\varSigma$. When $F = r - R(\theta, x, t)$, we get

$$\boldsymbol{u} \cdot \boldsymbol{n} = \boldsymbol{u} \cdot \frac{\boldsymbol{\nabla} F}{|\boldsymbol{\nabla} F|} = \frac{1}{|\boldsymbol{\nabla} F|} \frac{\partial R}{\partial t}. \tag{2.13}$$

2.3. *Energy equation for rigid motions of two fluids*

The disturbance equations given in §2.2 imply that

$$\frac{\mathrm{d}\mathscr{E}}{\mathrm{d}t} + \mathscr{D}[\hat{u}] = \langle \hat{u} \cdot \boldsymbol{n}([p_0] + 2HT) \rangle_\varSigma, \tag{2.14}$$

where

$$\mathscr{E}[\hat{u}] = \tfrac{1}{2}\langle p\hat{u}^2 \rangle \tag{2.15}$$

is the energy and

$$\mathscr{D}[\hat{u}] = \langle 2\mu D[\hat{u}] : D[\hat{u}] \rangle \tag{2.16}$$

is the dissipation. Moreover, making use of the transport theorem for surface areas (see, for example, (96.11) in Joseph 1976), we may write

$$\langle \hat{u} \cdot \boldsymbol{n}([p_0] + 2HT) \rangle_\varSigma = \langle \boldsymbol{u} \cdot \boldsymbol{n}[p_0] \rangle_\varSigma - \langle \boldsymbol{u}_0 \cdot \boldsymbol{n}([p_0] + 2HT) \rangle_\varSigma$$
$$+ T \left\{ -\frac{\mathrm{d}|\varSigma|}{\mathrm{d}t} + \int_{\partial\varSigma} \boldsymbol{U} \cdot \boldsymbol{\tau}\, \mathrm{d}l \right\}, \quad (2.17)$$

where $|\varSigma|$ is the area of $\varSigma$, $\boldsymbol{\tau}$ is the outward normal to $\partial\varSigma$, lying on $\varSigma$, and $\boldsymbol{U}$ is the velocity of a point of the contact line $\partial\varSigma$. under certain circumstances, to be specified in §2.5, we can express (2.17) as the time derivative of some potential $\mathscr{P}$, that is,

$$\langle \hat{u} \cdot \boldsymbol{n}([p_0] + 2HT) \rangle_\varSigma = -\frac{\mathrm{d}\mathscr{P}}{\mathrm{d}t}. \tag{2.18}$$

We may then write (2.14) as

$$\frac{\mathrm{d}}{\mathrm{d}t}(\mathscr{E} + \mathscr{P}) = -\mathscr{D}. \tag{2.19}$$

2.4. *Assumptions about the interface $\varSigma$*

We assume that the interface $\varSigma$ between the two fluids has a finite number of components; each of them is represented locally by a finite number of equations $r = R(\theta, x, \tau)$, where R is a continuously differentiable function, periodic in θ. These local charts also satisfy suitable continuity conditions at common points.

We also assume that the boundary $\partial\varSigma$ has measure zero in $\mathbb{R}^3$ as in the case of bubbles, drops and emulsions, or $\partial\varSigma$ has a finite number of components, say $\partial\varSigma = \partial\varSigma_A \cup \partial\varSigma_c$, where $\partial\varSigma_A$ lies on the endwalls at $x = \pm A$ and can be represented by a graph $r = R(\theta, \pm A, t)$ and where $\partial\varSigma_c$ lies on one of the cylinders and is composed of a finite number of contact lines, each of them with a graph of the form $x = \chi(R_i, \theta, t)$, where $i = 1$ or 2.

2.5. *Reduction of the interface terms*

We proceed now to the terms on the right-hand side of (2.17). These were computed by JRRN for the periodic problem and by C. Guillopé & D. D. Joseph for this paper (cf. Guillopé *et al.* (1987) for another application). We assume that $\varSigma$ is given by an equation $r = R(\theta, x, t)$ for $x_1(\theta, t) < x < A$, $0 \leqslant \theta < 2\pi$. The function R is continuously differentiable and periodic in θ. Here $\partial\varSigma_c$ is given by the $x = \chi(R_1, \theta, t) = x_1(\theta, t)$ where χ is continuously differentiable and periodic in θ and $\partial\varSigma_A$ is given by the curve $r = R(\theta, A, t)$.

Since $\langle \boldsymbol{u}_0 \cdot \boldsymbol{n} \rangle_\Sigma = 0$, we find that

$$\langle \boldsymbol{u}_0 \cdot \boldsymbol{n}[p_0] \rangle_\Sigma = \langle \boldsymbol{u}_0 \cdot \boldsymbol{n} R^2 \rangle_\Sigma \tfrac{1}{2}[\rho] \Omega^2 .$$

We define
$$I_1 = \langle \boldsymbol{u}_0 \cdot \boldsymbol{n} R^2 \rangle_\Sigma = -\Omega \int_0^{2\pi} \int_{x_1(\theta)}^A R_\theta R^3 \, \mathrm{d}x \, \mathrm{d}\theta ,$$

where $\boldsymbol{u}_0 = \Omega R \boldsymbol{e}_\theta$. Using Leibnitz's rule we find that

$$\frac{\mathrm{d}}{\mathrm{d}\theta} \int_{x_1(\theta)}^A R^4 \, \mathrm{d}x = 4 \int_{x_1(\theta)}^A R^3 R_\theta \, \mathrm{d}x - \frac{\mathrm{d}x_1}{\mathrm{d}\theta} R^4(\theta, x_1(\theta)) ,$$

and after integrating, using periodicity, find that $I_1 = 0$.

The calculation of $\langle \boldsymbol{u} \cdot \boldsymbol{n}[p_0] \rangle_\Sigma$ is similar. Since $\langle \boldsymbol{u} \cdot \boldsymbol{n} \rangle_\Sigma = 0$, we have

$$\langle \boldsymbol{u} \cdot \boldsymbol{n}[p_0] \rangle_\Sigma = \tfrac{1}{2} \Omega^2 [\rho] \langle \boldsymbol{u} \cdot \boldsymbol{n} R^2 \rangle_\Sigma .$$

Then, using (2.13) and $\mathrm{d}\Sigma = R|\boldsymbol{\nabla}F| \, \mathrm{d}\theta \, \mathrm{d}x$, we get

$$I_2 = \langle \boldsymbol{u} \cdot \boldsymbol{n} R^2 \rangle_\Sigma = \int_0^{2\pi} \int_{x_1(\theta)}^A R_t R^3 \, \mathrm{d}x \, \mathrm{d}\theta . \tag{2.20}$$

Since
$$\frac{\mathrm{d}}{\mathrm{d}t} \int_0^{2\pi} \int_{x_1(\theta, t)}^A R^4(\theta, x, t) \, \mathrm{d}x \, \mathrm{d}\theta = 4I_2 - \int_0^{2\pi} \frac{\partial x_1}{\partial t} R^4(\theta, x_1(\theta)) \, \mathrm{d}\theta$$

$$= 4I_2 - R_1^4 \frac{\mathrm{d}}{\mathrm{d}t} \int_0^{2\pi} x_1(\theta, t) \, \mathrm{d}\theta , \tag{2.21}$$

it follows now, from (2.21), that I_2 is the time derivative of some function and

$$\langle \boldsymbol{u} \cdot \boldsymbol{n}[p_0] \rangle_\Sigma = \frac{\mathrm{d}}{\mathrm{d}t} \left\{ \tfrac{1}{8} \Omega^2 [\rho] \left(\langle R^3 |\boldsymbol{\nabla}F|^{-1} \rangle_\Sigma + \int_{\partial\Sigma_c} \phi \, \mathrm{d}l \right) \right\} , \tag{2.22}$$

where
$$\phi = \pm R_i^3 \chi|_{r=R_i} \boldsymbol{t} \cdot \boldsymbol{e}_\theta , \quad i = 1, 2 ,$$

and $\boldsymbol{t}$ is the unit tangent vector to $\partial\Sigma_c$. In the expression for ϕ the sign is $+$ (resp. $-$) on the parts of $\partial\Sigma_c$ being on the right (resp. left) side of a component of fluid 1.

We turn next to the reduction of

$$\langle \boldsymbol{u}_0 \cdot \boldsymbol{n} 2HT \rangle_\Sigma = -T\Omega \int_0^{2\pi} \int_{x_1(\theta, t)}^A 2H R R_\theta \, \mathrm{d}x \, \mathrm{d}\theta , \tag{2.23}$$

using the formula
$$RR_\theta 2H = \frac{\partial}{\partial\theta} \left[-\frac{R(1+R_x^2)}{|\boldsymbol{\nabla}F|} \right] + \frac{\partial}{\partial x} \left[\frac{RR_x R_\theta}{|\boldsymbol{\nabla}F|} \right] ,$$

derived in JRRN. We may integrate this expression. The second term leads to

$$\int_0^{2\pi} \int_{x_1(\theta)}^A \frac{\partial}{\partial x} \left[\frac{RR_x R_\theta}{|\boldsymbol{\nabla}F|} \right] \mathrm{d}x \, \mathrm{d}\theta = \int_0^{2\pi} \left[\frac{RR_x R_\theta}{|\boldsymbol{\nabla}F|} \bigg|_A - \frac{RR_x R_\theta}{|\boldsymbol{\nabla}F|} \bigg|_{x_1} \right] \mathrm{d}\theta . \tag{2.24}$$

For the first term we use Leibnitz's rule

$$\frac{\mathrm{d}}{\mathrm{d}\theta} \int_{x_1}^A -\frac{R(1+R_x^2)}{|\boldsymbol{\nabla}F|} \, \mathrm{d}x = \int_{x_1}^A \frac{\partial}{\partial\theta} \left[-\frac{R(1+R_x^2)}{|\boldsymbol{\nabla}F|} \right] \mathrm{d}x + \frac{\partial x_1}{\partial\theta} \left[\frac{R(1+R_x^2)}{|\boldsymbol{\nabla}F|} \right]_{x_1} .$$

Since $R_1 = R(\theta, x_1(\theta))$ and $\partial x_1/\partial \theta = -R_\theta/R_x$, we have

$$\int_0^{2\pi} \int_{x_1}^{\Lambda} \frac{\partial}{\partial \theta} \left[-\frac{R(1+R_x^2)}{|\nabla F|} \right] dx\, d\theta = R_1 \int_0^{2\pi} \left[\frac{R_\theta}{R_x} \frac{1+R_x^2}{|\nabla F|} \right]_{x_1} d\theta. \tag{2.25}$$

Collecting results from (2.23), (2.24) and (2.25), we find that

$$\langle \boldsymbol{u_0} \cdot \boldsymbol{n} 2HT \rangle_\Sigma = -T\Omega \int_0^{2\pi} \left\{ \frac{R_x R_\theta R}{|\nabla F|} \bigg|_\Lambda + \frac{R_1 R_\theta}{R_x |\nabla F|} \bigg|_{x_1} \right\} d\theta. \tag{2.26}$$

We may re-express the second term on the right in terms of χ,

$$\frac{R_1 R_\theta}{R_x |\nabla F|} \bigg|_{x_1} = -\frac{R_1 \chi_\theta \chi_r}{|\nabla F|} \bigg|_{R_1}, \tag{2.27}$$

where $|\nabla F| = (1 + R_\theta^2/R^2 + R_x^2)^{\frac{1}{2}}$ in the first term on the right of (2.26) and $|\nabla F| = (1 + \chi_\theta^2/R_1^2 + \chi_r^2)^{\frac{1}{2}}$ in the second term, using (2.27).

Finally the calculation of $\boldsymbol{U} \cdot \boldsymbol{\tau}$ on Σ implies that

$$\int_{\partial \Sigma} \boldsymbol{U} \cdot \boldsymbol{\tau}\, dl = \int_0^{2\pi} \left\{ \frac{RR_x R_t}{|\nabla F|} \bigg|_\Lambda - \frac{R_1 \chi_r \chi_t}{|\nabla F|} \bigg|_{R_1} \right\} d\theta. \tag{2.28}$$

Let α_Λ be the angle between the interface Σ and the endwalls and α_c the angle between the interface Σ and the cylinders. Then

$$\left. \begin{aligned} \cos\alpha_\Lambda = \boldsymbol{n} \cdot \boldsymbol{e_x} = -\frac{R_x}{|\nabla F|}, \\ \cos\alpha_c = \boldsymbol{n} \cdot \boldsymbol{e_r} = \frac{\chi_r}{|\nabla F|}. \end{aligned} \right\} \tag{2.29}$$

After introducing (2.29) into (2.26) and (2.28) and collecting all the previous results, we find that

$$-\langle \hat{\boldsymbol{u}} \cdot \boldsymbol{n}([p_0] + 2HT) \rangle_\Sigma = \frac{d}{dt} \left\{ T|\Sigma| + \tfrac{1}{8}\Omega^2[\rho] \left(\left\langle \frac{R^3}{|\nabla F|} \right\rangle_\Sigma + \int_{\partial \Sigma_c} \phi\, dl \right) \right\}$$

$$+ T \int_0^{2\pi} \{ (R_t + \Omega R_\theta) R \cos\alpha_\Lambda|_{x=\Lambda} + (\chi_t + \Omega\chi_\theta) R_1 \cos\alpha_c|_{r=R_1} \}\, d\theta. \tag{2.30}$$

2.6. *The interface potential*

In order to reduce the interface terms (2.30) to potential form we assume that

(i) The contact angle at the interface on the endwalls depends only on the distance r from the contact line to the axis of the cylinder. (At two different points θ_1 and θ_2 at which $r_1 = r_2$, the contact angle will be the same.)

(ii) The contact angle at the interface on the cylinders depends only on the distance $\Lambda - x$ of the contact line to the end wall at $x = \Lambda$.

The form of the functional dependence will be explicitly discussed in §2.10.

The assumptions (i) and (ii) imply the existence of two functions $\psi_\Lambda(R)$ and $\psi_c(\chi)$ such that

$$\left. \begin{aligned} R\cos\alpha_\Lambda(R) = \psi_\Lambda'(R), \\ R_1 \cos\alpha_c(\chi) = \psi_c'(\chi). \end{aligned} \right\} \tag{2.31}$$

The reduction of (2.30) to a time derivative of a potential $\mathscr{P}$, using (2.31), is straightforward. We write

$$\int_0^{2\pi} \{(R_t + \Omega R_\theta)\, \psi'_A(R) + (\chi_t + \Omega \chi_\theta)\, \psi'_c(\chi)\}\, \mathrm{d}\theta$$

$$= \int_0^{2\pi} \frac{\mathrm{D}}{\mathrm{D}t}(\psi_A + \psi_c)\, \mathrm{d}\theta = \frac{\mathrm{d}}{\mathrm{d}t} \int_0^{2\pi} \{\psi_A(R) + \psi_c(\chi)\}\, \mathrm{d}\theta, \qquad (2.32)$$

where $\mathrm{D}/\mathrm{D}t = \partial/\partial t + \Omega\,\partial/\partial\theta$ is a derivative following rigid motion. The notations in (2.32) are slightly misleading; the integration is to be carried out on each and every contact line. We may write (2.32) as

$$\frac{\mathrm{d}}{\mathrm{d}t} \int_{\partial \Sigma} \psi\, \mathrm{d}l,$$

where
$$\psi = \boldsymbol{t} \cdot \boldsymbol{e}_\theta \begin{cases} \pm \psi_{\pm A}(R)|_{x=\pm A} & \text{on } \partial\Sigma_A, \\ \pm \psi_c(\chi)|_{R-R_i} & \text{on } \partial\Sigma_c \quad (i = 1, 2). \end{cases}$$

It now follows that $\mathscr{P}$ in (2.19) is given by

$$\mathscr{P} = T\left\{ |\Sigma| - \int_{\partial\Sigma} \psi\, \mathrm{d}l \right\} - \tfrac{1}{8}[\rho]\Omega^2 \left\{ \left\langle \frac{R^3}{|\nabla F|} \right\rangle_\Sigma + \int_{\partial\Sigma} \phi\, \mathrm{d}l \right\}. \qquad (2.33)$$

Finally we note that the working of the contact line cannot always be represented by a potential. The relation of the assumptions (i) and (ii) which lead to a potential and the classical ones in which contact angles or contact lines are fixed is obscure. We note, however, that these assumptions hold trivially for the case of a fixed line or a constant angle independent of position and, in general, whenever implicit relations of the form $f_1(\alpha, R) = 0$ or $f_2(\alpha, \chi) = 0$ are valid.

2.7. *Poincaré's inequality and the energy inequality*

Let $\boldsymbol{v}$ belong to a space X of square integrable solenoidal vectors defined in G which vanish on the solid parts of the boundary of G, or are periodic in x, with period $2A$, if the cylinders are infinitely long. Suppose further that the gradients of such functions are also square integrable in G where integration is in the sense (2.9). Such functions are said to lie in $H'(G)$ and they are automatically continuous in G, even across Σ, $[\boldsymbol{v}] = \boldsymbol{O}$. Each such $\boldsymbol{v}$ satisfies Korn's inequality

$$\langle |\boldsymbol{v}|^2 \rangle \leqslant 2k \langle |\boldsymbol{D}[\boldsymbol{v}]|^2 \rangle, \qquad (2.34)$$

for some positive constant k. Since

$$2\langle |\boldsymbol{D}[\boldsymbol{v}]|^2 \rangle = \langle |\nabla \boldsymbol{v}|^2 \rangle + \langle |\mathrm{div}\, \boldsymbol{v}|^2 \rangle,$$

and $\mathrm{div}\, \boldsymbol{v} = 0$, the constant k is Poincaré's constant.

Using (2.34) we may establish that

$$\mathscr{D}[\boldsymbol{v}] \geqslant 2\tilde{\lambda}\mathscr{E}[\boldsymbol{v}], \quad \forall \boldsymbol{v} \in X, \qquad (2.35)$$

where
$$\tilde{\lambda} = \frac{\min[\mu_1, \mu_2]}{k \max[\rho_1, \rho_2]}. \qquad (2.36)$$

The inequality (2.35) holds for connected configurations as well as for bubbles, drop and emulsions.

It now follows from (2.35) and (2.11) that

$$\frac{\mathrm{d}}{\mathrm{d}t}(\mathscr{E}+\mathscr{P}) \leqslant -2\tilde{\lambda}\mathscr{E}. \tag{2.37}$$

2.8. *Integrability of the energy*

Integrating (2.37) from $t = 0$ to t, we find that

$$\mathscr{E}(t)+\mathscr{P}(t) = \mathscr{E}(0)+\mathscr{P}(0)-\int_0^t \mathscr{D}(\tau)\,\mathrm{d}\tau \leqslant \mathscr{E}(0)+\mathscr{P}(0)-2\tilde{\lambda}\int_0^t \mathscr{E}(\tau)\,\mathrm{d}\tau.$$

It follows that

$$2\tilde{\lambda}\int_0^t \mathscr{E}(\tau)\,\mathrm{d}\tau \leqslant \mathscr{E}(0)+\mathscr{P}(0)-\mathscr{E}(t)-\mathscr{P}(t). \tag{2.38}$$

Let us suppose that $\mathscr{P}(\cdot)$ is bounded below on the set of allowed interfaces. In fact, if G is a bounded region, $\mathscr{P}(\cdot)$ is bounded from below. In unbounded domains $\mathscr{P}(\cdot)$ need not be bounded below. In a bounded domain we could centrifuge all the heavy fluid to the outer cylinder wall. In an unbounded domain we would centrifuge a certain amount of liquid of the inner rod before reaching some equilibrium in which the potential is bounded.

If $\mathscr{P}(\cdot)$ is bounded below as a functional on the set of interfaces, $\mathscr{E}(t)$ and $\mathscr{D}(t)$ are integrable and

$$\lim_{t\to\infty}[\mathscr{E}(t)+\mathscr{P}(t)] < +\infty.$$

We proved that $\mathscr{E}(t)$ tends to zero in the sense of integrability and we assume that $\mathscr{E}(\infty) = 0$.

2.9. *Minimum of the potential*

Let us consider the limit configuration $[\mathscr{E}(\infty), \mathscr{P}(\infty)]$; since $\mathscr{E}(\infty) = 0$, this is a rigid motion and

$$\mathscr{P}(\infty)-\mathscr{P}(0) = \mathscr{E}(0)-\int_0^\infty \mathscr{D}(\tau)\,\mathrm{d}\tau. \tag{2.39}$$

Clearly $\mathscr{P}$ decreases in every transformation for which the right-hand side of (2.39) is negative. We may find disturbances $\hat{u}$ at $t = 0$, for any Σ_0, such that $\mathscr{E}(0)/\mathscr{D}(0)$ is arbitrarily small. For these

$$\mathscr{P}(\infty)-\mathscr{P}(0) < 0. \tag{2.40}$$

It follows that all configurations that give rise to $\mathscr{P}$ different than $\mathscr{P}(\infty)$ are unstable and that

$$\mathscr{P}(\infty) = \lim_{t\to+\infty} \mathscr{P}(t) = \min_{\Sigma\in\mathscr{S}} \mathscr{P}[\Sigma] \tag{2.41}$$

where $\mathscr{S}$ is the set of allowable interfaces (see §2.4 and JRRN).

Finally, we note that critical points of $\mathscr{P}$ corresponds to steady rigid motions for which the normal-stress equation (2.2) holds;

$$[p_0]+2HT = 0,$$

and the boundary conditions (2.31) are Euler equations for the minimization problem defined by (2.41) subject to the constraints of constant volumes for the two liquids.

We may state the results just proved as follows: assume that the contact-angle assumptions (i) and (ii) hold. Then (*a*) rigid motions are almost stable in the sense

that the energy of disturbances is integrable on $(0, \infty)$ and (b) the stable configurations associated with rigid motion minimize $\mathscr{P}$ in $\mathscr{S}$.

2.10. *Relation between the contact line and the contact angle*

Assumptions (i) and (ii) are equivalent to assuming a functional relation in which the contact angle is determined by its position on the contact line. (We could also state equivalent conditions in which the contact line is determined by the angle: say, the contact line does not move.) Precisely, such a functional relation is a differentiable map $\mathscr{F}$ between the set $\mathscr{C}$ of contact lines and the set $\mathscr{A}$ of contact angles. For instance, in the case of endwall ($x = \pm \Lambda$), $\mathscr{C}$ is the space of 2π-periodic functions $R = R(\theta)$, which are continuously differentiable with values in $[R_1, R_2]$; $\mathscr{A}$ is the space of 2π-periodic functions, which are continuous with values in $[-\tilde{R}_2, R_2]$, and

$$\mathscr{F}: \quad \begin{matrix} \mathscr{C} & \to & \mathscr{A} \\ R & \to & R \cos \alpha_A \end{matrix}$$

$$\text{contact line} \quad \text{contact angle}.$$

The equation of Young and Dupré is given by

$$\mathscr{F}(R) = CR,$$

where $C(= \cos \alpha_A)$ is a fixed constant in $[-1, 1]$. Assumption (i) is equivalent to the more general equation $\mathscr{F}(R, \theta) = \phi_{\pm A}[R(\theta)]$, where $\phi_{\pm A}$ is a given absolutely continuous function from $[R_1, R_2]$ into $(-R_2, R_2)$.

The assumption that there is a functional relation between the contact line and the contact angle is not inconsistent with our observations about the relation between the angle and the position on silicone-oil rollers rotating in water on a Plexiglas rod (figure 13). The angle $\alpha_c(x)$ between the interface and the rod at the line of contact $x = \chi$ is a monotonic function of $x - x_s$ where x_s is the static angle which is finally achieved after transients have decayed and the potential is minimized. The contact line moves about 1 cm in 3 days, so that the velocity of the contact line is negligible and the angle does not depend on the velocity.

2.11. *Spatially periodic connected interfaces*

In this section we shall assume that the interface is a graph

$$r = R(\theta, x),$$

periodic, with period 2π in θ, and period $2\pi/\alpha = 2\Lambda'$ in x. We shall show that either $R = d$, where d is the mean radius of R or the minimizing solution touches the axis at $r = 0$. This means that we get periodic arrays of drops and bubbles which have contact lines on the inner rod or make tangent contact with the wetted rod.

The analysis of stable configurations starts from the expression (2.33) for $\mathscr{P}$. It is assumed that there are no end plates and that $R(\theta, x) \geqslant a$, with possibly flat tangents at $R = a$. The contact-line potentials ϕ and ψ are put to zero. Then we may write (2.33) as

$$\mathscr{P} = \int_0^{2\pi/\alpha} \int_0^{2\pi} \{T[R^2 + R_\theta^2 + R^2 R_x^2]^{\frac{1}{2}} - \tfrac{1}{8}[\rho]\,\Omega^2 R^4\}\,\mathrm{d}\theta\,\mathrm{d}x, \tag{2.42}$$

where

$$d^2 = \int_0^{2\pi/\alpha} \int_0^{2\pi} R^2\,\mathrm{d}\theta\,\mathrm{d}x. \tag{2.43}$$

In the analysis that follows we shall work with a potential $\mathscr{M}$, differing from $\mathscr{P}$ by terms that are independent of R.

3. Solutions of the minimum problem

3.1. *Mathematical formulation of the minimum problem*

Joseph *et al.* (1985), showed that rigid motions of two liquids between concentric cylinders of radius R_1 and R_2 are stable to spatially periodic disturbances of arbitrary amplitude and that the stable interface $r = R(\theta, x)$ minimizes the potential

$$\mathcal{M} = T(([R^2 + R_\theta^2 + R^2 R_x^2]^{\frac{1}{2}})) - \tfrac{1}{8}[\rho]\Omega^2(([R^2 - d^2]^2)), \tag{3.1}$$

where T is the interfacial tension, $[\rho] = \rho_1 - \rho_2$ where ρ_1 is the density of the inner fluid, Ω is the angular velocity of the two fluids, d^2 is the spatial average of R^2

$$((R^2)) = ((d^2)), \tag{3.2}$$

where

$$((\cdot)) = \int_0^{2\pi/\alpha} \mathrm{d}x \int_0^{2\pi} (\cdot)\,\mathrm{d}\theta,$$

and $2\pi/\alpha$ is the wavelength in the x-direction. When the heavy fluid is outside, $[\rho] < 0$, $\mathcal{M}$ is minimized by $R(\theta, x) = d$ whenever

$$J = -\frac{[\rho]\Omega^2 d^3}{T} > 4. \tag{3.3}$$

If $J < 4$, the minimizing solution is not of constant radius. The volume constraint (3.2) eliminates solutions of constant radius other than d. When $J = 0$, the interface is a surface of constant mean curvature, spherical, independent of θ. We shall study the θ-independent solutions.

We measure all lengths in units d, setting $r = R(x)/d$, where x and α are dimensionless. Then there is a new $\mathcal{M}$ which is the old one divided by Td and such that

$$\mathcal{M} = ((r[1 + r_x^2]^{\frac{1}{2}} + \tfrac{1}{8}J[r^2 - 1]^2)), \tag{3.4}$$

where

$$((r^2 - 1)) = 0. \tag{3.5}$$

We seek to minimize $\mathcal{M}$ among periodic functions $r(x)$, in the class $C^1(x)$ satisfying (3.5). To do this, we introduce a Lagrange multiplier λ and seek the minimum of $\mathcal{M} + 2\lambda((r^2 - 1))$ among periodic $C^1(x)$ functions $r(x)$. The Euler equation for this problem is

$$\frac{1 + r'^2 - r''r}{(1 + r'^2)^{\frac{3}{2}}} + [\tfrac{1}{2}J(r^2 - 1) - \lambda]r = 0. \tag{3.6}$$

We may find a first integral of (3.6) by following a change of variables first introduced by Beer (1869). Consider the interface curve formed in the intersection of the axisymmetric interface and a plane through the axis $r = 0$ of revolution. The coordinates in this plane are (x, r) and the angle between the interface curve $r = r(x)$ and x is ψ. We define

$$v = \cos\psi, \quad 0 \leqslant v^2 \leqslant 1. \tag{3.7}$$

Then

$$r' = \tan\psi = \frac{(1 - v^2)^{\frac{1}{2}}}{v},$$

and

$$r'' = \frac{\mathrm{d}r'}{\mathrm{d}r}r' = \frac{\mathrm{d}\tan\psi}{\mathrm{d}r}\tan\psi = -\frac{1}{v^3}\frac{\mathrm{d}v}{\mathrm{d}r}.$$

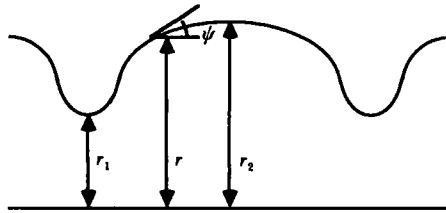FIGURE 1. Solution (I) of unduloid type.
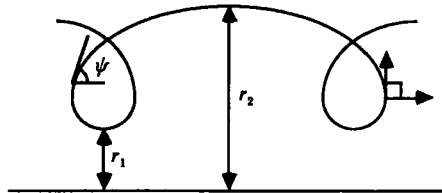
FIGURE 2. Solution (II) of nodoid type.

The Euler equation (3.6) becomes

$$\frac{\mathrm{d}}{\mathrm{d}r}(rv) + \tfrac{1}{2}J\,r^3 - \mu r = 0,\qquad(3.8)$$

where $\mu = \tfrac{1}{2}J(1+\lambda)$ is as yet undetermined and

$$v(r) = -\tfrac{1}{8}J\,r^3 + \tfrac{1}{2}\mu r - \frac{\beta}{r},\qquad(3.9)$$

where β is a constant of integration.

The solution (3.9) is to be associated with an interface profile satisfying $r' = (1-v^2)^{\frac{1}{2}}/v$ and the volume constraint

$$((r^2-1)) = 4\pi \int_{r_1}^{r_2} \frac{(r^2-1)\,v}{(1-v^2)^{\frac{1}{2}}}\,\mathrm{d}r = 0.\qquad(3.10)$$

We may find all the axisymmetric solutions of our problem $v(r(x))$ governed by (3.9). There are solutions (I) of unduloid type, $v = \cos\psi$ (see figure 1), if

$$\text{for any } r, \quad 0 \leqslant v(r) \leqslant 1,\qquad\text{(I)}$$

and solutions (II) of nodoid type (see figure 2) if

$$\text{there exists } \hat{r}\,|\,v(\hat{r}) < 0.\qquad\text{(II)}$$

The angle between the interface curve and the x-axis is ψ and $r' = \tan\psi$. An unduloid is a surface of constant mean curvature, $J = 0$, which is generated by the focus of a rolling ellipse. A nodoid is a surface of constant mean curvature, $J = 0$, which is generated by the focus of a rolling hyperbola.

3.2. *Analysis of the minimum problem*

It is convenient to replace the parameters (μ, β) with (r_1, r_2), the minimum and maximum values of $r(x)$ (see figures 1, 2). Since $r'(r_1) = r'(r_2) = 0$ we have $v(r_1) = v(r_2) = 1$ and, using (3.9), we find that

$$\left.\begin{aligned}
\tfrac{1}{8}Jr_i^4 - \tfrac{1}{2}\mu r_i^2 + r_i + \beta &= 0 \quad (i = 1, 2) \\
\beta &= r_1 r_2 \left[\tfrac{1}{8}J r_1 r_2 - \frac{1}{r_1 + r_2}\right], \\
\tfrac{1}{2}\mu &= \tfrac{1}{8}J(r_1^2 + r_2^2) + \frac{1}{r_1 + r_2}, \\
rv &= \tfrac{1}{8}J(r^2 - r_1^2)(r_2^2 - r^2) + \frac{r^2 + r_1 r_2}{r_1 + r_2}.
\end{aligned}\right\} \quad (3.11)$$

Moreover, since $r' = (1 - v^2)^{\frac{1}{2}}/v$,

$$x(r) = \int_{r_1}^{r} \frac{v(\zeta)}{(1 - v^2(\zeta))^{\frac{1}{2}}} \, \mathrm{d}\zeta. \quad (3.12)$$

The period of periodic solutions is given by

$$\lambda = 2 \int_{r_1}^{r_2} \frac{v(\zeta)}{(1 - v^2(\zeta))^{\frac{1}{2}}} \, \mathrm{d}\zeta.$$

Solutions (I) of the unduloid type have $0 \leqslant v \leqslant 1$. The constraint from above leads us to

$$(r - r_1)(r_2 - r) \left[\tfrac{1}{8}J(r + r_1)(r + r_2) - \frac{1}{r_1 + r_2}\right] \leqslant 0.$$

Hence
$$J \leqslant \frac{8}{(r + r_1)(r + r_2)(r_1 + r_2)}, \quad (3.13)$$

for all $r \in [r_1, r_2]$. When $r = r_2$ (3.13) reduces to

$$J \leqslant \frac{4}{r_2(r_1 + r_2)^2}. \quad (3.14)$$

In the problem treated by JRRN the fluid is confined by cylinders of radius R_1 and R_2. Hence $r_1 \geqslant R_1/d$ and $r_2 \geqslant 1$, so that if

$$J \leqslant \frac{4}{[1 + R_1/d]^2}, \quad (3.15)$$

then J satisfies (3.14). The largest possible J for a solution of unduloid type is obviously $J = 4$. When $J \geqslant 4$, the only solution of our minimum problem is the interface of constant radius $r(x) = 1$.

The other condition $v \geqslant 0$ for a solution of unduloid type leads us to the inequality

$$J \geqslant -\frac{8(r^2 + r_1 r_2)}{(r_1 + r_2)(r_2^2 - r^2)(r^2 - r_1^2)}, \quad (3.16)$$

for all $r \in [r_1, r_2]$. Let us choose $r \in [r_1, r_2]$ so as to make the right-hand side of (3.16) as large as possible; i.e.

$$\left.\begin{aligned}
r^2 &= (r_1 r_2)^{\frac{1}{2}} (r_1 + r_2 - (r_1 r_2)^{\frac{1}{2}}), \\
J &\geqslant -\frac{8}{(r_1 + r_2)^2 (r_2^{\frac{1}{2}} - r_1^{\frac{1}{2}})^2} = -\theta.
\end{aligned}\right\} \quad (3.17)$$

Solutions of type (I) are possible only when J satisfies the inequalities (3.14) and (3.17).

If $J < -\theta$, solutions of type (I) are not possible and we get solutions (II) of nodoid type. After introducing the new variables into (3.4) and (3.5), we seek the minimum of

$$\mathcal{M} = 4\pi \int_{-\frac{1}{2}\pi}^{\frac{1}{2}\pi} \left[\frac{r^2 + \frac{1}{8}J(r^2-1)^2 \, rv(r)}{(g(r))^{\frac{1}{2}}} \right] \mathrm{d}\theta \tag{3.18}$$

subject to the volume constraint

$$0 = 4\pi \int_{-\frac{1}{2}\pi}^{\frac{1}{2}\pi} \left[\frac{(r^2-1)\,rv(r)}{(g(r))^{\frac{1}{2}}} \right] \mathrm{d}\theta, \tag{3.19}$$

where

$$g(r) = (r+r_1)(r+r_2) \left\{ \left[\frac{1}{r_1+r_2} - \frac{1}{8}J(r^2+r_1 r_2) \right]^2 - \frac{1}{64}J^2 r^2(r_1+r_2)^2 \right\} \tag{3.20}$$

is positive, and $r(\theta)$ is defined by

$$r = \frac{1}{2}(r_1+r_2) + \frac{1}{2}(r_2-r_1)\sin\theta. \tag{3.21}$$

The volume constraint gives r_2 as a function of r_1, $0 \leqslant r_1 \leqslant 1$.

The form of the solution just given is new and is particularly convenient for numerical calculations. It is necessary to distinguish between constrained and unconstrained minima. In the unconstrained problem we minimize $\mathcal{M}$ as r_1 varies. Numerical calculations of Preziosi (1986) show that these minimizers cross the axis with $r'(0) = \infty$. Therefore, the unconstrained minimizers are either bubbles ($J > 0$) or drops ($J < 0$). The distance $x(r)$, (3.12), between the minimum radius r_1 and the radius $r(x)$ is now given by

$$x(r) = \int_{-\frac{1}{2}\pi}^{\phi} \frac{v(y)y^{\frac{1}{2}}\,\mathrm{d}\theta}{\left\{ (r_2+y) \left[\left(\frac{1}{8}J y^2 - \frac{1}{r_2} \right)^2 - \frac{1}{64}J^2 r_2^2 y^2 \right] \right\}^{\frac{1}{2}}}, \tag{3.22}$$

where $y = \frac{1}{2}r_2(1+\sin\theta)$ and $\phi = \arcsin[2r/r_2 - 1]$. The wavelength λ is $2x(r_2)$, where $x(r_2)$ is the distance between the maximum and minimum values of r. When $r = r_2$, $\phi = \frac{1}{2}\pi$. Tables of values $r_2(J)$ and $\lambda(J)$ for unconstrained minimizers are given by Preziosi (1986). When $J \geqslant 4$, the minimizing interface has constant radius. The period $\lambda(J)$ of the minimizing solutions with $J > 0$ is monotonically from a sphere $J = 0$ to a cylinder $J \geqslant 4$. When $-5.42285 \leqslant J < 4$ the solutions are of unduloid type. When $-8.18834 < J < -5.42285$, the minimizing solutions are of nodoid type (II). When $J < -8.18834$, there are no axisymmetric minimizers.

Another form of the solution just given, in which it is implicitly assumed from the start that the minimizers cross the axis, can be found in Rosenthal's (1962) study of rotating bubbles and Chandrasekhar's (1965) study of rotating drops. These authors prescribe volume rather than the mean radius. The condition on non-existence of axisymmetric minimizing drops $J < -8.18834$ was first given by Chandrasekhar who uses a drop parameter $-\frac{1}{8}Jr_2^3 = [\rho]\Omega^2 a^3/8ST$, where α is the maximum radius of the drop. He mentions the possibility of toroidal figures of equilibrium (see figure 3). These figures were first discussed by Rayleigh (1914) and studied extensively by Ross (1968). Toroidal figures of equilibrium at large negative values of J might be interpreted to mean that there are no locally stable flows with heavy fluid inside; all
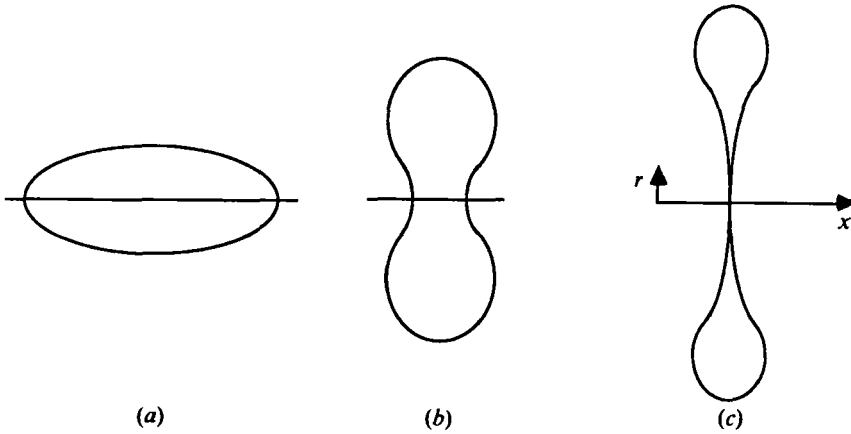
FIGURE 3. Schematic drawing of minimizing solutions. Minimizing solutions touch the axis with a perpendicular tangent. (a) Solutions of unduloid type are convex, $4 \geqslant J \geqslant -5.42285$. (b) Solutions of nodoid type have a point of inflexion $-5.42285 \geqslant J \geqslant -8.18834$. (c) Limiting (toroidal) form of the solution for $J = -7.583908$.

of the heavy liquid has been centrifuged to the outer cylinder giving rise to robustly stable flows with $J > 4$.

If we prescribe a contact angle θ at the rod at $r = a$, then (3.8) leads to

$$r(v-1) = (r_2-r)f(r, \theta, r_2, a, J),\qquad(3.23)$$

where

$$f \overset{\text{def}}{=} \tfrac{1}{8}J(r^2-a^2)(r_2+r) - \frac{r_2-a\cos\theta}{r_2^2-a^2}(r_2+r) + 1 \leqslant 0,\qquad(3.24)$$

because $r_2 > r$ and $v = \cos\psi$. Equation (3.23) is a first-order differential equation, $\cos\psi = (r'^2+1)^{-\frac12}$ which is to be integrated from $x = x_1$, where $(r, r') = (a, \tan\theta)$ to $x = x_2$ where $r' = 0$. f is a cubic in r and it has two points where $\partial f/\partial r = 0$, one of which is negative. It follows that when $a \leqslant r \leqslant r_2$, f is a decreasing function of r with a maximum at $r = a$, or f has a single minimum in $a < r < r_2$ and f is a maximum at the end points a or r_2. We can verify that $f(a, \theta, r_2, a, J) \leqslant 0$ automatically, and $f(r_2, \theta, r_2, a, J) \leqslant 0$ if and only if

$$J \leqslant 4\frac{(r_2^2+a^2-2r_2a\cos\theta)}{r_2(r_2^2-a^2)^2}.$$

For long bubbles, $v-1 \sim -\tfrac12\psi^2$ and $r_2-r \sim \psi l$ and $f(r, \theta, r_2, a, J) \to 0$ with ψ implying the equality in (3.24) for long bubbles. We can compute surface tension T when the bubble is long and r_2 and $\cos\theta$ are known.

3.3. *Periodic solutions, drops and bubbles*

Solutions that cross the axis may be regarded as limiting cases of periodic solutions. Then we get a periodic array of drops $(J < 0)$ or bubbles $(J > 0)$ lined up with their centres on the axis of rotation. If we put a rod of radius a at the centre of the array, the resulting configuration would assume the form of an array of rollers. When the periodic solution is viewed as an array of drops or bubbles, r_2 is one radius of the drop and $\tfrac12\lambda$ is the other. The sphere with $r_2 = (3/2)^{\frac13}$ corresponds to a volume of $\pi\sqrt{6}$, which is the volume of a right circular cylinder of unit radius and height $2r_2$. It is also of interest to briefly consider the mean curvature

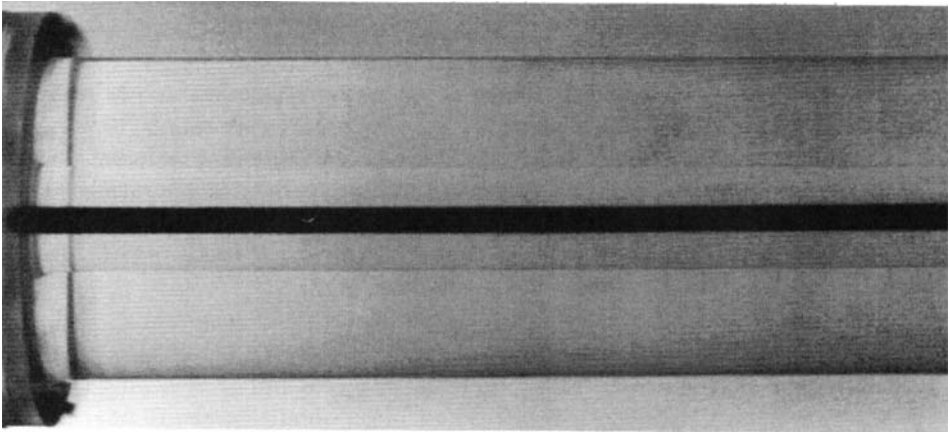$$H(r) = [v(r)\,r]'/2r = \tfrac18J(r_2^2-2r^2)+1/r_2$$

FIGURE 4. Cylindrical interface between 1000 cSt silicone oil and water when $J = 4.5$.
The radius of rod is 0.24 cm.

at the equator $r = 0$, $H(0) = \frac{1}{8}r_2^2 J + 1/r_2$, or at the poles $H(r_2) = -\frac{1}{8}r_2^2 J + 1/r_2$ of the rotating drop or bubble. The curvature at the equator is negative when $J \leqslant -8/r_2^3$ corresponding to solutions (II) of nodoid type.

It is useful to distinguish bubbles and drops by a dynamic criterion. Bubbles will elongate along their central rotating axis as Ω is increased. Drops contract under the same conditions. Using this criterion we suggest that the terminology oil 'drops' rotating in water, as in Plateau (1863) and in the experiments described in §§6.1 and 6.2 is precise.

In the case of bubbles $J > 4$ cannot be achieved because the bubbles will elongate as Ω is increased in such a way that the effective mean radius,

$$d = \left\{ \frac{4T}{[\rho]\Omega^2} \right\}^{\frac{1}{3}},$$

is a decreasing function of Ω. In our experiments using end plates and density matching to achieve microgravity, we prevent elongation and achieve a constant radius $R = d$ when $J > 4$, as in figure 4.

Leslie (1985) has solved the problem of rotating bubble shapes in a low-gravity environment. His drop can contact endwalls that are perpendicular to the axis of rotation. He applies the condition of constant contact angle (cf. §2.10) at the endwalls. He does not use density matching to achieve microgravity but instead does the experiment in a free-falling aircraft.

The presence of a central rod alters the dynamics of bubbles and drops in certain ways which will be specified in due course. For now it will suffice to call the reader's attention to figure 6 which shows small effects on bubbles, and to figures 7–10, which show large effects on 'drops' in air.

3.4. *All the solutions with J < 4 touch the cylinder*

Minimizing solutions that cross the axis of rotation will certainly touch the inner cylinder. The prediction that solutions with $J < 4$ will touch the cylinder is completely consistent with experiments. The cylinder-touching solutions that are observed are of two types: (i) the interface between the two fluids intersects the cylinder at lines of contact, as shown in figures 5, 6, and 13; and (ii) the interface between the two fluids makes a tangent contact with the wetted rod at $r = a$ as shown in figures 7–11. The physical mechanisms embodied in the difference between

(i) and (ii) are associated with fundamental problems of adhesion and cohesion not considered here.

The effects of capillarity at lines of contact should be considered for solutions of type (i), as in (3.23); but if a/r_2 be small, the effects of capillarity at contact lines will then also be small. The comparison between theory and experiment shown in §5.1 shows that contact-line effects are local even in cases when the interfacial tension is large; say when a is small compared with the bubble radius. In the other case (ii), with tangent contact, and no contact line, we acknowledge a constraint on our variational problem by looking for periodic solutions with troughs which touch the cylinder at $r = a$. This also works well (see figures 7–11).

3.5. *Critical remarks about stability theory*

The fact that realized solutions with $J < 4$ touch the cylinder is a motivation for remarks that are meant to be critical of current ideas about the study of stability of the flow of two fluids. When there is one fluid, there is a unique stable flow at low Reynolds numbers. When there are two fluids, there can be many configurations, even at zero Reynolds number. In the case of rigid motions, heavy fluid outside or inside and even nested sequences of drops and bubbles are possible. Different solutions can be realized in nature. So we have not got a unique solution to study but perhaps an infinity of such solutions (see JNB for examples). If we choose one of these and show instability, we eliminate one placement, but we have to study all the others. So with two fluids the identification of a basic flow and the study of its stability cannot be separated.

As an example of the considerations just discussed we note that Yih (1960) studied the problem of stability of a film of liquid rotating in air. He treated this problem in the linearized approximation, and studied the stability of rigid motions with a free surface of constant radius with gravity neglected. Naturally these constant-radius interfaces are unstable because J is negative. Rigid motions, with negligible gravity, are stable and can be obtained easily in experiments (see §§5.3 and 5.4) but the free surface cannot have a constant radius.

4. Experiments with heavy fluid outside – the spinning rod tensiometer

The case $J > 0$ corresponds to centrifuging, with heavy fluid outside, and $0 < J < 4$ is the domain corresponding to rigid rotation of bubbles whose long dimension increases monotonically from that corresponding to a sphere at $J = 0$ to an infinitely long cylinder of ever smaller diameter as $J \to 4$. Strictly speaking rigid rotation is possible only when the Froude-number criterion (2.4) is satisfied, $\Omega^2 d \gg 2g$. This criterion is independent of $[\rho]$. If $[\rho]$ is small we may have

$$|J| = \left| \frac{[\rho]\,\Omega^2 d^3}{T} \right| < 4 \qquad (4.1)$$

for values of Ω such that gravity is negligible.

The spinning rod tensiometer (US Patent 4 644 782) is a device for measuring interfacial tension between different liquids. This device competes with various spinning drop tensiometers (see Rosenthal 1962; Princen, Zia & Mason 1967). The rod and the drop tensiometers are designed to work under conditions of negligible gravity in which (2.4) and (4.1) hold simultaneously.
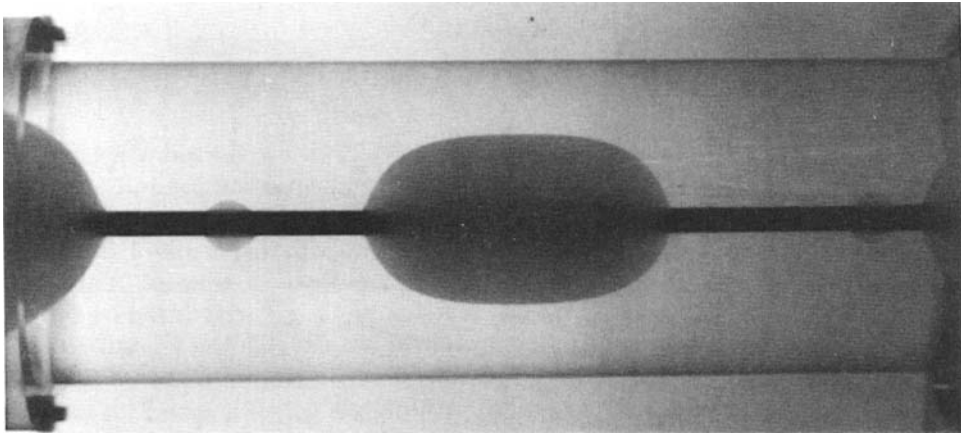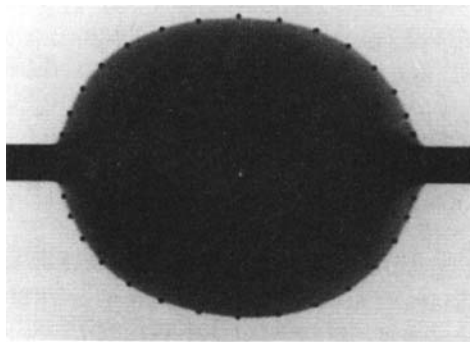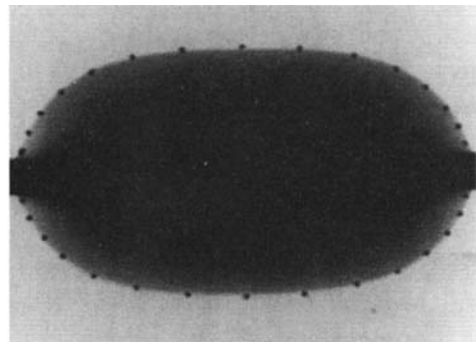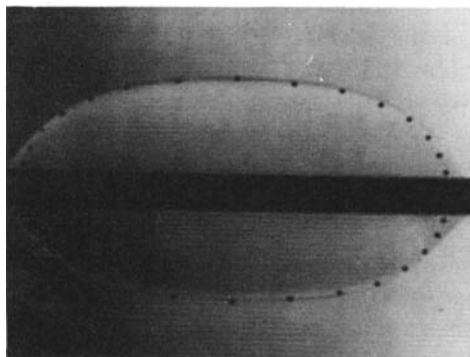
FIGURE 5. Array of bubbles of 95% silicone oil (12500 cSt) dyed with 5% castor oil ($\rho = 0.974$, $T = 20.5$) in water. $J = 1.87$ for the central bubble and 0.05 for the small ones. The radius of the aluminium rod is 0.24 cm.
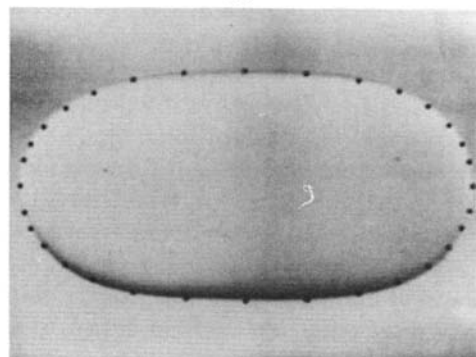

(a)

(b)

(c)

(d)

FIGURE 6. Numerical comparison. The dots are theory computed numerically (see (3.22)) neglecting the contact-line potential. The rod radius is 0.24 cm. (a) Bubble of 95% silicone oil (12500 cSt) dyed with 5% castor oil ($\rho = 0.974$, $T = 20.5$) in water when $J = 0.72$. (b) Bubble of 95% silicone oil (12500 cSt) dyed with 5% castor oil ($\rho = 0.974$, $T = 20.5$) in water when $J = 1.87$. (c) Bubble of silicone oil (1000 cSt, $\rho = 0.967$, $T = 22.1$) in water when $J = 2$. (d) Bubble of silicone oil (1000 cSt, $\rho = 0.967$, $T = 22.1$) in water when $J = 2$ without inner rod.

The working formula $f = 0$ (3.24) for the spinning rod tensiometer may be replaced with the working formula $J = 4/r_2^3$ for the spinning drop tensiometer when

$$\frac{1}{r_2^3} \left| \frac{r_2^2 + a^2 - 2r_2 a \cos \theta}{r_2 (r_2^2 - a^2)^2} - 1 \right| = \frac{2x \cos \theta + x^4 - 3x^2}{1 + x^2 - 2x \cos \theta} \overset{\text{def}}{=} g(x, \cos \theta) \ll 1,$$

where $x = a/r_2$, $g(0, \cos \theta) = g(x, \frac{1}{2}(3 - x^2)) = 0$. We may ignore the rod when a is small, r_2 is large or the contact angle at the rod is near to the angle on the bubble without the rod at the same radius.

The shape of rotating bubbles does not depend on whether a small rotating rod pierces the central axis of the bubble, except near lines of contact. This lack of sensitivity of shape on rod is partially controllable, the capillarity is reduced in small rods and may be reduced by using rods of different material and coated rods.

The experimental apparatus used to obtain the results reported here is a cylindrical container of Plexiglas with inner radius 3.6 cm, of length 24.5 cm, closed at each end. A rod may be inserted along the central axis. The rods are attached rigidly to the cylinder and all the parts rotate together as a rigid body. We used aluminium rods of radius 0.24 cm and 0.5 cm and a Plexiglas rod of radius 1.25 cm. A photograph of the cylindrical interface which appears whenever $J > 4$, shown as figure 4, will aid the reader in visualizing the cylinder apparatus.

The liquids used in our experiments were water, Castor oil, Soybean oil and 20, 1000 and 12500 c.p. silicone oils. The densities of these liquids are 1, 0.960, 0.922, 0.949, 0.967, 0.975 respectively. The small density difference greatly reduces perturbing effects due to gravity. The effects of gravity can be reduced to negligible levels with $|J| < 4$ when the density differences are < 0.1 and $d < 1$ cm, as in our experiments. If we suppose that $\Omega^2 d = 2gk$ for $k \gg 1$, then (4.1) requires that $[\rho] d^2 2gk < 4T$. Under these conditions we always get centrifuged configuration with heavy fluid outside, $[\rho] < 0$.

Solutions of permanent form, periodic in x, with heavy fluid outside ($0 < J < 4$), were never observed. Instead of periodic solutions we found isolated bubbles of light liquid centred on the rod. When $J > 4$, we get a cylindrical interface which is modified by capillarity at the endwalls. The effects of capillarity are smaller when $J - 4 > 0$ is larger. When J is reduced from above to below 4, the interface deforms continuously until points at the interior touch the axis. At this point we see some changes in the topology of the interface. The fluid may rupture into bubbles separated from the heavy liquid outside by well-defined contact lines. This depends on energetic considerations associated with the two fluids and the rods. The configuration of permanent form which we see most frequently when $0 < J < 4$ is like that shown in figure 5 in which small bubbles and large bubbles both appear.

We define d for an isolated bubble as the radius associated with a right circular cylinder of the same length and volume. It follows that there are different J values for small and large bubbles rotating with the same Ω. This is why the small bubbles are almost spherical and the large ones are elongated.

Agreement between theory and experiment is demonstrated in figure 6. The dots represent theory with capillarity neglected. The value of the interfacial tension may be selected to make theory and experiment agree for one value of Ω. The same interfacial tension then gives agreement for other values of Ω. In figure 6 (a, b) we can compare the agreement between theory and experiment for two different values of Ω, with one T. Figure 6 $(a–c)$ shows that capillarity is a small effect. This was true for all the cases we studied, even the worst-case situation, comparing a free bubble to a captured bubble, using the same interfacial tension, exhibited in figure 6 (c, d).

Very rapid measurements of surface tension may be obtained using elongated bubbles with aspect ratios greater than 6 by assuming that $J = 4$. More detailed comparison of theory with observed shapes leads to values of the interfacial tension T.

Some of the advantages enjoyed by the spinning rod tensiometer over various spinning drop tensiometers currently used are (1) the rod captures the bubble, eliminating the position problem; (2) the captured bubble is stable if small enough, eliminating the stability problem; (3) the rod reduces the spin-up time from hours to minutes; and (4) the cylinder-plus-rod device is simple and cheap and has a potential for high precision.

5. Experiments with heavy fluid inside – coating flows

We did experiments with heavy fluid inside, 'drop' experiments, of a special kind, coating aluminium and Plexiglas rods rotating in air with oil. With air outside, $[\rho] = \rho$ is not small and gravity can be important. The coating liquids used in our studies were STP, 1000 and 6000 P silicone oils. The viscosity of STP is about 100 P. The dynamics that we have observed are not inconsistent with the observations of Moffatt (1977) of films of golden syrup (80 P) rotating in air. Our study complements Moffatt's in carefully examining the axial structure of the rotating films as well as the azimuthal variations. We are interested in demonstrating that the shapes of the films are largely determined by minimizing the potential expressing energies associated with centripetal acceleration and surface tension, even when gravity is not negligible.

The apparatus used in these experiments is nearly identical with that used in the experiments of Moffatt (1977). A layer of liquid was first coated on the cylinder by rotating it while partially immersed in a trough; the roller was then raised from the trough while still rotating. The coating films achieved in this way could be maintained indefinitely. The films undergo many different transitions as flow parameters are changed. We used three different rods: two aluminium rods with radius and length 1.02, 30 cm and 1.42, 45 cm respectively and one Plexiglas rod with radius and length 2.04, 30 cm. The material and length of the rods is not important. The liquids coated the entire rod along its whole length.

All the fluids mentioned in the last paragraph are sticky. Once the rod is coated with these fluids, it stays coated; dry patches do not develop. This means that contact-line conditions are inappropriate for such coating flows. We are then obliged to reconsider the implications of the fact that in unconstrained problems the minimizing solutions cross the axis when $J < 4$. In the case of sticky coats on rotating rods we have a constrained variational problem in which we require that if the interface touches the rod it will do so with a flat angle of contact at touching points. In fact all the realized solutions touch the rod in just this way (see figures 7, 9, 10 and 11).

An oil which sticks on solids immersed in one fluid need not stick when immersed in another fluid. Silicone oil sticks to Plexiglas rods rotated in air, but not in water (see figures 12–14) even though silicone oil preferentially wets Plexiglas.

Some gross features of rod-touching oil films rotating in air may be explained as follows. Uniform coats are unstable and undulations begin to develop along the rod. Moffatt (1977) gave a heuristic argument which explains why this instability should not equilibrate until the troughs of the wavy interface touch the cylinder. In this

argument we neglect surface tension and suppose that a liquid is rotating in air with $p = p_a$ or $r = R(\theta, x, t)$. Then

$$p - p_a = \tfrac{1}{2}\rho(r^2 - R^2)\,\Omega^2,$$

and the pressure under any bump is less than the pressure at the side of the bump. In the absence of countervailing forces the pressure deficit would exaggerate the bump, with largest pressure gradients along lines from the point at the base of the bump where $p - p_a$ is minimum. This pressure gradient pulls in the sides of the bump, exaggerating bumpiness. This heuristic argument does not require axisymmetry; it works as well for bumps as for rings. The same argument works without change whenever the heavy fluid is inside, $[\rho] > 0$. When the speeds are low, axisymmetric wavy solutions with troughs that touch the cylinder minimize the interface potential (see §5.2). It is nearly impossible to pass fluid from one wave to another. Further increases in the angular velocity lead to increases in the amplitude of the undulations and length of the troughs touching the cylinders. These features are evident in figures 7–14 of this paper and figures 5 and 6 of Moffatt (1977). The undulations are then isolated from one another and it is not useful to think of periodic (in x) solutions, however periodic they may appear to be. Periodicity can be more closely simulated when the viscosity of the coating fluid is smaller. In this case the transfer of fluid from one undulation to another, which is required to maintain periodicity against disturbances, is enhanced. It may be useful to think of the undulations as rotating drops constrained by tangent contact at the rod. From these explanations the reader should understand why long very thin films separate rotating drops making tangent contact, whether or not the array of drops appears to be periodic.

5.1. *Effects of gravity*

The analysis of Moffatt (1977) and the analysis and experiments of Preziosi & Joseph (1988) show that the effects of gravity on coated rods rotating in air are small when

$$S h_0^2 \ll 1, \quad S = \frac{ga}{\nu\Omega}, \tag{5.1}$$

where h_0 is the maximum value of the film thickness $h(\theta, x)$. We approach rigid motion when the film thickness is small and the viscosity is large. When $S h_0^2 = 1$, the rate of rotation of the rod is insufficient to maintain the load and some of the fluid will drop off the rod, as honey drops off a slowly rotating knife. At this critical condition the maximum surface velocity is approximately $\tfrac{1}{2}\Omega a$ (see Moffatt 1977, equation 13). The removal of fluid reduces h_0 so that $gah_0^2/\nu\Omega \leqslant 1$. If we now increase Ω, and bifurcation does not occur, we may satisfy (5.1) with an axisymmetric figure.

5.2. *Computation of the interface shape of rigidly rotating coating flows making tangent contact at the rod*

We first determine d in the plane $\theta = \tfrac{1}{2}\pi$. Given Ω, T, $[\rho]$, we may then compute J. We next seek that solution of our equation that makes a tangent contact at the rod, at $r_1 = a/d$. With d and r_1 given, r_2 is uniquely determined and (3.12) may be used to compute the shape of the free surface. This procedure produces good agreement with experiments (cf. figure 7, and figure 4a, b in Preziosi & Joseph 1988).

5.3. *Bifurcation of coating films to non-axisymmetric shapes*

The problem of shapes of interfaces between fluids that rotate rigidly without shear, when gravity is neglected, is determined by a balance of the capillary force against
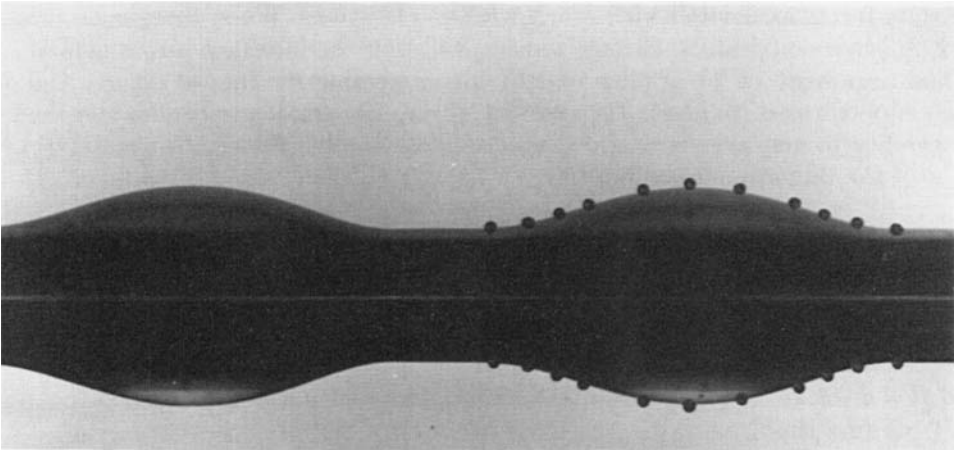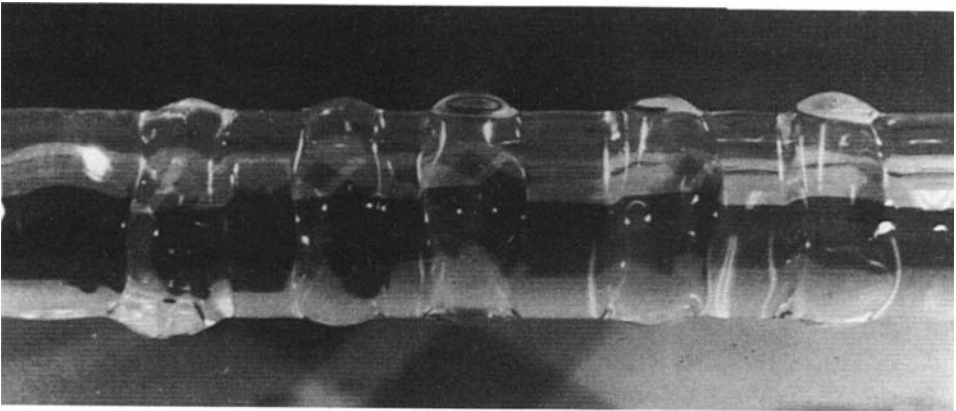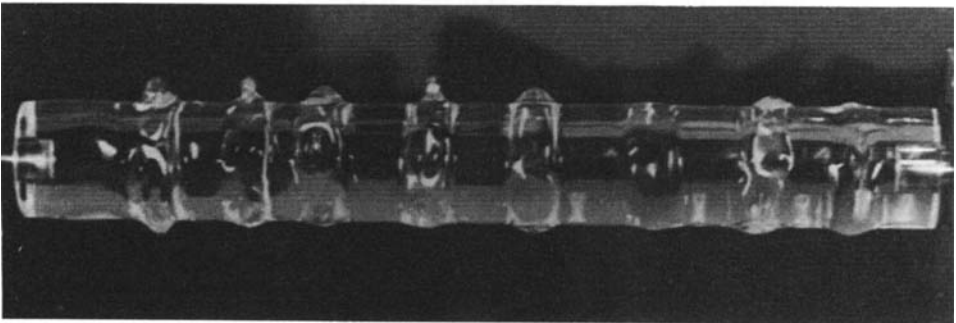
FIGURE 7. The rod is coated with STP and is rotating in air with $J = -0.95$, $a/d = 0.74$ and $Sh_0^2 = 0.57$. The dots compare the observed shape with the axisymmetric drop that has a tangent contact at $r = a$. The shape of this axisymmetric figure is determined by the method of §5.2.

(a)

(b)

FIGURE 8. (a) Bifurcated non-axisymmetric solutions on rings of 6000 P silicone oil in air on a 2.04 cm rotating Plexiglas rod. (b) Instability of the bifurcated rings at a higher rotation rate.

pressure forces associated with centripetal accelerations. When there is no rotation, and no other constraints, surface tension will pull the interface into a sphere.

The argument of §4 applies equally to axisymmetric shapes (rings) and non-axisymmetric ones (bumps). The stability of rings for small amplitudes and their loss of stability to non-axisymmetric shapes at large amplitudes can be argued from the form of the dimensionless potential.

$$\tilde{\mathscr{P}} = ((-1)) + (([[(1+\varDelta)^2\,(1+\varDelta_x^2)+\varDelta_\theta^2]^{\frac{1}{2}}])) + \tfrac{1}{8}J(([2\varDelta+\varDelta^2]^2)),\tag{5.2}$$

where

$$J = \frac{(\rho_2-\rho_1)\,d^3\varOmega^2}{T},\tag{5.3}$$

and $R = d+\delta$; $(\delta, x, 1/\alpha)$ are made dimensionless with d and $\varDelta = \delta/d$. Since $((R^2)) = ((d^2))$ we find that

$$((2\varDelta+\varDelta^2)) = 0,\tag{5.4}$$

and the average deviation $\varDelta = -1+R/d$ from zero must be negative if the volume of the two fluids is preserved. The linearized form of (5.2) is

$$\left.\begin{aligned}\tilde{\mathscr{P}} &= \tfrac{1}{2}(([J-1]\,\varDelta^2+\varDelta_x^2+\varDelta_\theta^2)),\\((\varDelta)) &= 0.\end{aligned}\right\}\tag{5.5}$$

The minimum value of (5.5) is taken for $\varDelta_\theta = 0$ and very long waves, small wavenumbers α. Such disturbances are compatible with $((\varDelta)) = 0$ and $\varDelta_x \to 0$. Since $\varDelta$ is periodic in θ, with period 2π, $\varDelta_\theta \neq 0$ leads always to a finite contribution to $\tilde{\mathscr{P}}$. If we suppose that the heavy fluid is inside, then $J < 0$ and if $\varOmega$ is also large the second term in (5.2) decreases when $(([2\varDelta+\varDelta^2]^2)) = ((\varDelta^4+4\varDelta^3-8\varDelta))$ increases. For large $|\varDelta|$ this term is dominated by $\varDelta^4$. The largest values of $|\varDelta|$ occur at points at which $R > d$, $\varDelta > 0$, $\varDelta_x = 0$, because, on the average (5.4) requires $\varDelta < 0$. Near these points we get larger values of $(1+\varDelta_x^2)(1+\varDelta)^2$. As $\varOmega$ increases the maximum values at which $\delta = R-d > 0$ get larger and $\varDelta_x$ grows near such points. When the positive of δ are sufficiently large we pay a greater price by increasing $\varDelta_x$ than by increasing $\varDelta_\theta$ values. Then bifurcation occurs.

The argument just given shows that non-axisymmetric solutions will form on rings $R-d > 0$ of relatively short length. Such bifurcation on narrow rings can be seen in figure 8 and in figures 6(a) and 9(b) of Moffatt (1977).

It is also obvious, from the way that the θ-variations appear in (5.10), that the first non-axisymmetric solution to bifurcate, as $\varOmega$ is increased, will have a first-mode azimuthal periodicity corresponding to an eccentric ring. Write $\varDelta(x,\theta) = \varDelta^0(x)+\varDelta'(x)\cos n\theta$ and linearize for small $\varDelta'(x)$. Then, $\varDelta_\theta^2 = n^2\varDelta'^2(x)\sin^2 n\theta$. This is smallest for $n = 1$. Repeated bifurcation of non-axisymmetric solutions leads to ever higher modes of azimuthal periodicity.

The bifurcation of axisymmetric figures of equilibrium to first-mode, eccentric figures is a robust and possible generic phenomenon, readily observed on nearly every type of coating film, whether rotating in air or in water (see figures 9, 10 and 14(a)). The same type of first-mode azimuthal periodicity was observed in the experiments of Plateau (1863, see his figure 4) as the first bifurcation of the olive-oil drop coating the rotating disk in an alcohol–water mixture. This type of instability does not make sense for free rotating drops since the central axis of a free drop is not fixed in space.
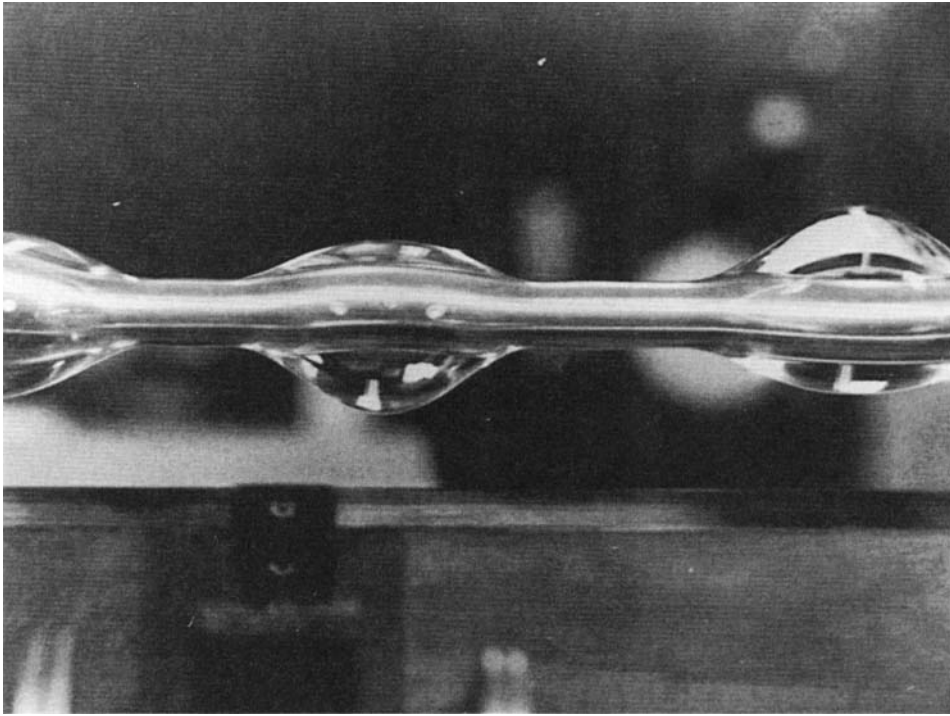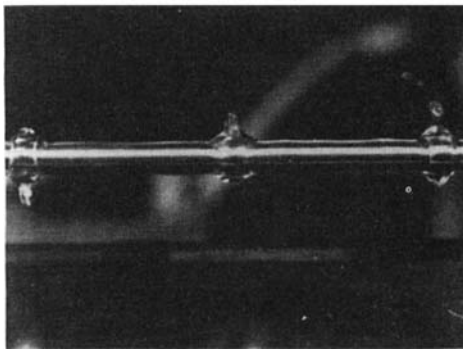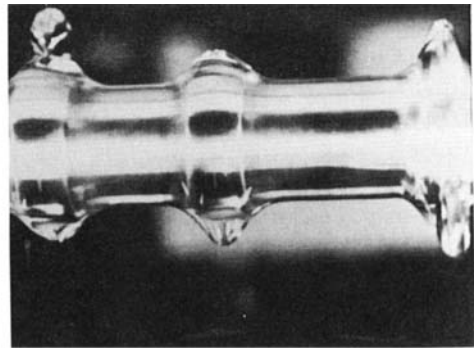
FIGURE 9. Silicone oil (6000 P) on a 1.02 cm radius aluminium rod rotating in air at 21.9 r.p.m. The lobes rotate much more slowly: left to right 15, 18.8 and 13.7 r.p.m. respectively.

| (a) | (b) |

FIGURE 10. The 6000 P silicone oil is thrown off radially. The effects of gravity are negligible. The configuration is nearly steady in a rotating coordinate system. (a) $\Omega = 99.15$ r.p.m., $a = 1.02$ cm; (b) $\Omega = 31.76$ r.p.m., $a = 2.04$ cm. The surface velocities of the three rings (b) from the left to right are 31.41, 31.57 and 31.53 r.p.m. respectively.

Non-axisymmetric one-lobed shapes were analysed by Brown & Scriven (1980) for a drop captured between two rotating disks. These calculations showed that higher-lobed shapes between disks, like those reported by Plateau and here are indeed unstable. First-mode, eccentric figures, like the shape of drops rotating on a rod, can even be explained within the context of static figures. In his observations of static capillary bridges, Plateau observed such a bifurcation when the end plates confining
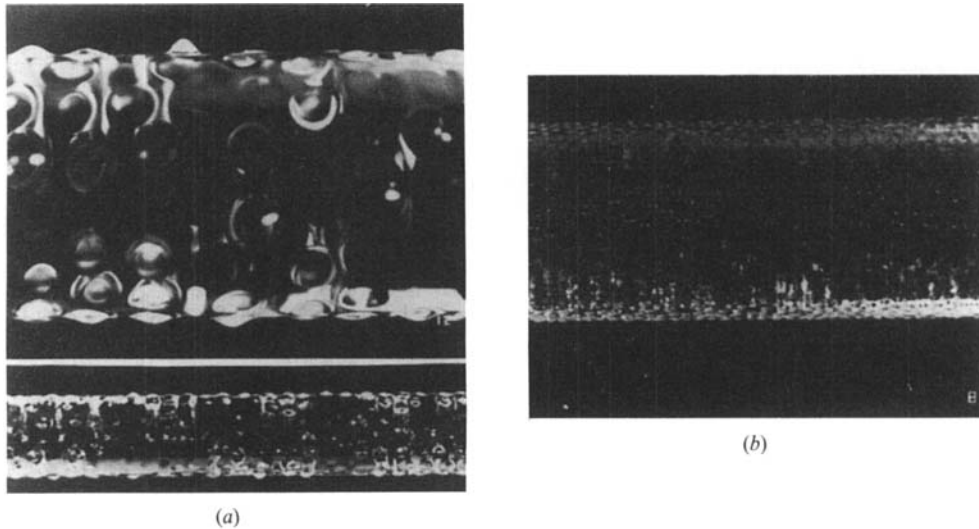
FIGURE 11. Pendant drops of 6000 P silicone oil in air on a rod of radius 2.04 cm. The motion is perfectly steady in a rotating coordinate system. Gravity is negligible. (a) $\Omega = 500$ r.p.m. (b) 1000 r.p.m.

the neutrally buoyant fluid were brought sufficiently close to one another. This reduces the wavelength, as in the case of rotating drops, until the price paid by further decrease of the axial wavelength in minimizing the potential is greater than that for bifurcation into the first mode. Russo & Steen (1986) have recently analysed this bifurcation in the context of static figures.

5.4. *Intrinsically steady and unsteady coating flows*

Flows that are steady in laboratory coordinates can be achieved when Ω is small. For larger values of Ω, these flows are unsteady in every coordinate system. For very large values of Ω, thin films rotate rigidly and are steady in a rotating coordinate system.

It is impossible to maintain an interface of constant radius on a film of liquid coating a rod rotating in air. If the coat is thick gravity can be very effective in creating a large secondary motion, with gravity opposing the motion on one side of the film and supporting it on the other. The effects of gravity are greater when there is more liquid on the rod. For fixed volume of liquid, the effects of gravity are diminished when the viscosity is increased; however, more liquid will remain on the rod at given speed when the liquid is more viscous (cf. §4). The two effects compete. At low speeds an equilibrium is established with a 'lopsided' configuration as in figure 4(b) of Preziosi & Joseph (1988) which is steady in laboratory coordinates.

As the speed of rotation is increased the out-of-roundness begins to increase and also to rotate relative to laboratory coordinates. This is a manifestation of bifurcation to a mode-one azimuthal variation, but it is slightly masked by out-of-roundness due to gravity (see figure 9). Such solutions are intrinsically unsteady. At the same time the crest of the waves grow and rings develop, in the manner shown in figure 10 and in figure 7 and 8 of Moffatt (1977).

When the coating fluid is very viscous and the coating film is thin, the effects of gravity will be diminished, as shown in figure 10. Thin films can be created by centrifuging away excess fluid. If the speed of rotation is further increased, more
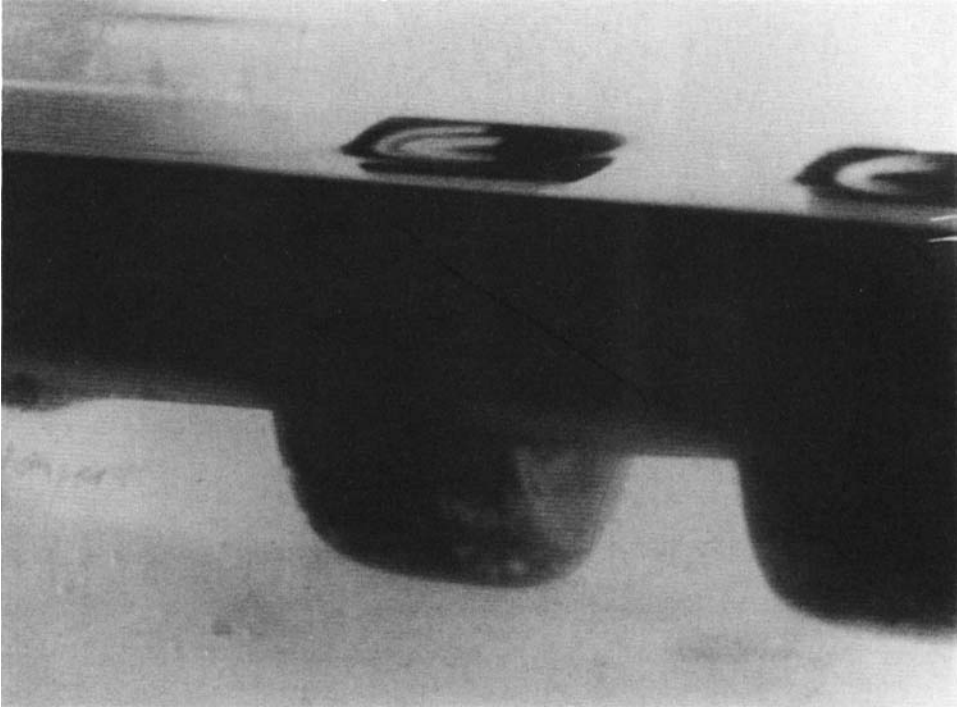
FIGURE 12. STP roller immersed in water, lubricated by water everywhere, poking its head into air. The shape of this roller is nodoid like (see figure 3).

liquid will be flung off the rod. At very high speeds most of the fluid is thrown off the rod. Gravity has nothing to do with 'throwing off' because ejected particles of fluid are flung out radially. An equilibrium is reached in which there are pendant drops on a rotating rod. These are shown in figure 11.

Pendant drops are a symmetry-breaking bifurcated solution of our coating film. They tend to form on the rings of earlier solutions with successive rows staggered so that the drops in one row lie in the interstice of the next row. This induces the diamond symmetry shown in the figures. The pendant drops are like those that might develop under gravity on a moist ceiling with an effective gravity equal to $\Omega^2 a$.

6. Rollers

This section is partly an addendum to the two papers of Joseph *et al.* (1984, 1986) in which we try to explain what is observed there using what we have learned here.

6.1. *Rods coated with oil rotating in water: rollers and drops*

We shall discuss two fluid situations in which both fluids do not rotate rigidly. We are interested in situations in which oil coats the rod, and both the rod and the attached oil rotate in water. If the oil is sufficiently viscous, it will rotate with the rod as a rigid body. This rigid rotation was achieved in all our experiments with STP, 1000 and 6000 P silicone oil. We have obtained, but do not give here, the boring data that show that the oil masses rotate rigidly. It is also of interest to consider cases in which the rigid rotating rod plus oil is immersed partly in water and partly in air, as in figure 12. The oil bodies that rotate as rigid wheels in fluids of smaller viscosity
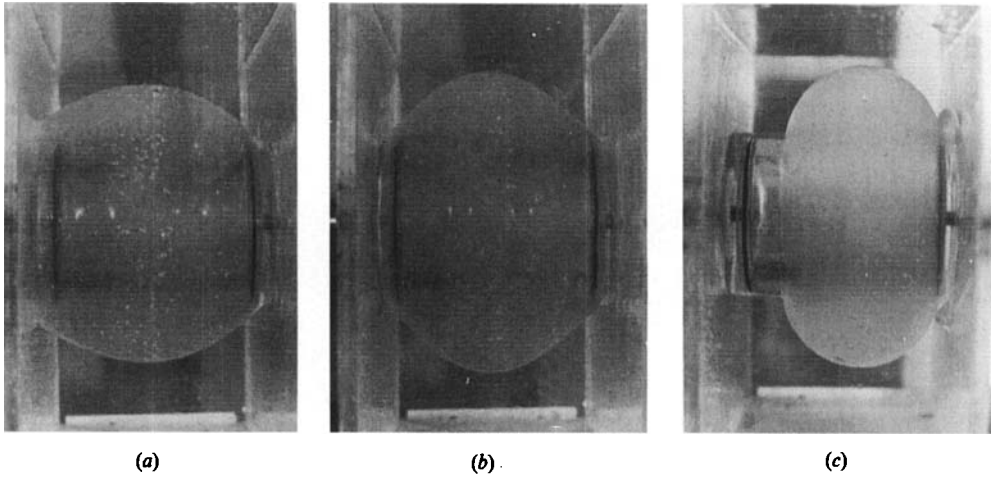
FIGURE 13. Detachment of rollers from the sidewalls. The diameter and length of the Plexiglas cylinder are 5.7 cm and 10.8 cm respectively. The roller of silicone oil (1000 P, $\rho = 0.997$) rotates in water. (a) $\Omega = 0.75$ rad/s. The roller is attached to the sidewalls. (b) $\Omega = 1.19$ rad/s. The speed is increased. The wavelength of the roller decreases as in a rotating drop and the roller detaches from the wall. The critical Ω for detachment is 1.14 rad/s. (c) $\Omega = 1.19$ rad/s, but three days later, the minimizing solution appears to have the form required for a rotating drop. In fact, we get qualitative agreement between the theory given in §6.2 and the experiments if we imagine the roller to be a drop of density ρ (water) $- \rho$ (oil) > 0. We call attention to the change in the contact angle with the position of the contact line.

have been called rollers (see JNB). The dynamical problem posed by the experiments of Plateau (1863) in which olive-oil drops on a disk were rotated in an alcohol–water mixture also falls in this frame.

We shall say that oil masses rotating rigidly in water are analogous to drops. This contradicts the static definition of a drop which is when the heavy fluid is inside ($J < 0$). Rollers and Plateau's 'drops' have the light oil inside ($J > 0$). We call these 'static bubbles' drops because they act like drops when they are rotated, the length λ along the axis of rotation of these drops or rollers shortens and the maximum radius r_2 increases as the angular velocity Ω is increased. We have not reconciled the obvious difference between the static and dynamic definitions of a drop.

It is necessary to say that the cases under discussion here differ from those in §5 in that the water is confined to a stationary box and the water does not rotate rigidly, though the oil does.

Plateau (1863) reports that he observed an unstable toroidal figure of equilibrium, stable for a time, when he increased the rate of rotation of the disk driving the oil drop in the density-matched bath of alcohol and water. The sequence seen by him is like that shown in figure 3(b, c), a solution of nodoid type valid for rotating drops.

In figure 12 we show fat rollers of STP rotating rigidly, lubricated everywhere by water, immersed in water at the bottom and with their tops poking into air. Gravity enters into the dynamics of these rollers; the water pushes up on the bottom and the air pulls down with a much bigger pull at the top. These gravity effects are stabilizing, tending to stabilize otherwise unstable toroidal drops of equilibrium. Figure 14 of JNB is another even better example of a nodoid-type solution of toroidal shape modified by gravity.
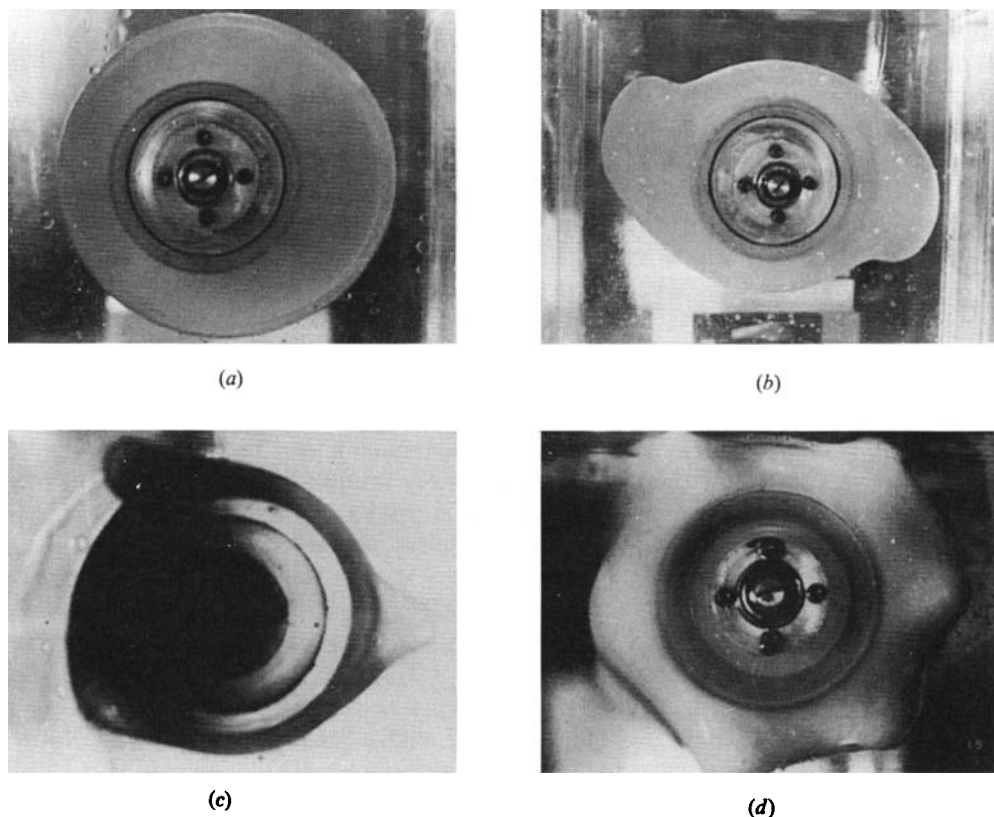
FIGURE 14. Bifurcated configurations of silicone oil in water. Only the one-lobed figure is stable in our experiments; the other figures eventually degenerate into a single lobe. This is consistent with predictions given by Brown & Scriven (1980) for a related problem. The one- and two-lobed structures resemble figures 4 and 8 sketched in the work of Plateau (1863). (*a*) One lobe, $\Omega = 0.47$ rad/s; (*b*) two lobes, $\Omega = 0.83$ rad/s; (*c*) three lobes, $\Omega = 1.49$ rad/s; (*d*) six lobes, $\Omega = 3.18$ rad/s.

Photographs of interpenetrating rollers immersed partly in water and partly in air have been exhibited in JNB. The dynamics of these rollers are partly explained by drop dynamics. The first dramatic dynamic event in the formation of inter-penetrating rollers is that a sheet of water fingers through the STP joining the two rotating cylinders, splitting the STP into more or less thick cylindrical films, each on its own cylinder. These films develop the same type of undulations as are characteristic for films rotating in air. The undulations grow in the manner consistent with rotating drops. However their growth is blocked by the presence of the second cylinder and they form square rollers which are consistent with minimizing a drop potential subject to a unilateral constraint.

6.2. *Sidewall detachment of single rollers*

Sidewall detachment of single rollers was described by JNB and by JRRN. An attempt to describe underlying dynamics was made by JRRN, who say that the most interesting feature of the dynamics leading to the formation of rollers is the fracturing of the viscous liquid at some critical level of the stress. In this process the roller breaks away from the sidewall and relieves the high stress associated with no

slip at the sidewall. So in the final, stable dynamics, rollers are lubricated by water and air on all sides. The rollers rotate nearly as rigid bodies because they are so viscous. The stability of rollers, as our analysis suggests, depends on the fact that the density stratification is such as to prevent the centrifuging of the roller.

Several major points in the foregoing analysis must be revised in the light of our work here. The first revision does away with the notion of a critical stress. The sidewall detachment takes place as a kind of instability associated with a critical angular velocity. Photographs of this instability are exhibited as figure 15 of JNB (1984).

We now want to explain sidewall detachment in terms of drop dynamics. The roller will attach to the sidewall at all values of Ω below a critical one for which the length of the drop with contact at $r = a$ is equal to the distance between the sidewalls. For larger values of Ω this length is less than the distance between sidewalls. This line of thought appears to explain qualitatively all of our observations of sidewall detachment (see figure 13). The foregoing explanation can be made quantitative under the hypothesis that the oil roller completely immersed in water is the same as a roller with an effective density equal to the density of water minus the density of oil, like a light drop rotating in air without gravity. We have not been able to justify this hypothesis mathematically, but it is consistent with the measurements reported in the caption of figure 13.

We close this discussion of oil masses rotating in water with some remarks about bifurcation. Again it is necessary to revise JRRN in which it was said, 'This instability [to non-axisymmetric disturbances] is associated with viscous shearing, which becomes important at higher speeds and with a possible unstable distribution of angular momentum'. We want to de-emphasize the effects of viscous shearing and to emphasize the intrinsic instability. The arguments given in §5.3 apply here. In general we get bifurcated sequences in the order of increasing azimuthal periodicity, first $n = 1$ as in figure 14(a), then $n = 2$ as in figure 14(b). Some higher values of n are shown in figure 14(c, d). The viscous shearing is very important for the bifurcated structures shown in figure 14(c), but it is not the cause of the bifurcation. Our observations of bifurcating sequences reproduced the sketches shown in figures 4–8 of the celebrated treatise of Plateau (1863) and in photographs by Wang *et al.* (1981). The same sort of phenomenon, bifurcation of rotating drops into non-axisymmetric shapes in qualitative agreement with theory, although the theory does not acknowledge the outer fluid, was reported by Wang *et al.* (1981).

This paper is dedicated to James Serrin for his 60th birthday.

REFERENCES

BEER, A. 1869 *Einleitung in die Matematische Theorie der Elastizität und Capillaritat*. Leipzig: A. Gresen Verlag.

BROWN, R. A. & SCRIVEN, L. E. 1980 The shape and stability of rotating liquid drops. *Phil. Trans. R. Soc. Lond.* A 297, 51–79.

CHANDRASEKHAR, S. 1965 The stability of a rotating liquid drop, *Proc. R. Soc. Lond.* A 286, 1–26.

GUILLOPÉ, C., JOSEPH, D., NGUYEN, K. & ROSSO, F. 1987 *J. Mec. Théor. Appl.* **6**, (5).

JOSEPH, D. D. 1976 *Stability of Fluid Motions II*. Springer.

JOSEPH, D. D., RENARDY, Y., RENARDY, M. & NGUYEN, K. 1985 Stability of rigid motions and rollers in bicomponents flows of immiscible liquids, *J. Fluid Mech.* **153**, 151–165.

JOSEPH, D. D., NGUYEN, K. & BEAVERS, G. S. 1984 Non-uniqueness and stability of the configuration of flow of immiscible fluids with different viscosities. *J. Fluid Mech.* **141**, 319–345.

JOSEPH, D. D., NHUYEN, K. & BEAVERS, G. S. 1986 Rollers. *Phys. Fluids.* **29**, 2771.

LESLIE, F. 1985 Measurements of rotating bubble shapes in a low-gravity environment. *J. Fluid Mech.* **161**, 269–280.

MOFFATT, K. 1977 Behaviour of a viscous film on the outer surface of a rotating cylinder. *J. Méc.* **16**, 651–673.

PLATEAU, J. A. F. 1863 Experimental and theoretical researches on the figures of equilibrium of a rotating liquid mass withdrawn from the action of gravity. *Annual Report of the Board of Regents and Smithsonian Institution, Washington, DC*, pp. 270–285.

PREZIOSI, L. 1986 Selected topics in the mechanics of two fluids and viscoelastic media, Ph.D. thesis, University of Minnesota.

PREZIOSI, L. & JOSEPH, D. D. 1988 The run-off condition for coating and rimming flows. *J. Fluid Mech.* (to appear).

PRINCEN, H. M., ZIA, I. Y. Z. & MASON, S. G. 1967 Measurements of interfacial tension from the shape of a rotating liquid drop. *J. Colloid Interface Sci.* **23**, 99–107.

RAYLEIGH, LORD 1914 The equilibrium of revolving liquid under capillary force. *Phil Mag.* **28**, 161–170.

ROSENTHAL, D. K. 1962 The shape and stability of a bubble at the axis of a rotating liquid. *J. Fluid Mech.* **12**, 358–366.

ROSS, D. K. 1968 The shape and energy of a revolving liquid mass held together by surface tension. *Austral. J. Phys.* **21**, 823–835.

RUSSO, M. J. & STEEN, P. H. 1986 Instability of rotund capillary bridges to general disturbances, experiment and theory. *J. Coloid Interface Sci.* **113**, 154–163.

WANG, T. G., TAGG, R., CAMMACK, L. & CROONQUIST, A. 1981 Non-axisymmetric shapes of a rotating drop in an immiscible system. In *Proc. 2nd Int. Colloq. on Drops and Bubbles* (ed. D. H. LeCroisette), pp. 203–213, NASA-JPL.

YIH, C. S. 1960 Instability of a rotating liquid film with a free surface. *Proc. R. Soc. Lond.* A **258**, 63–86.